January 2008

Measurement and Computational Modeling of the Mechanical Properties of Parallel Strand Lumber

Russell S. Winans
University of Massachusetts Amherst, rwinans@student.umass.edu

MEASUREMENT AND COMPUTATIONAL MODELING OF THE MECHANICAL PROPERTIES OF PARALLEL STRAND LUMBER

A Thesis Presented

by

RUSSELL WINANS

Submitted to the Graduate School of the
University of Massachusetts Amherst in partial fulfillment
of the requirements for the degree of

MASTER OF SCIENCE IN CIVIL ENGINEERING

September 2008

Civil and Environmental Engineering

MEASUREMENT AND COMPUTATIONAL MODELING OF THE MECHANICAL PROPERTIES OF PARALLEL STRAND LUMBER

A Thesis Presented

by

RUSSELL WINANS

Approved as to style and content by:

Sanjay R. Arwade, Chair

Peggi Clouston, Member

Thomas Lardner, Member

Richard Palmer, Department Head
Civil and Environmental Engineering

To my parents Patricia and Steven Winans

ABSTRACT

MEASUREMENT AND COMPUTATIONAL MODELING OF THE MECHANICAL PROPERTIES OF PARALLEL STRAND LUMBER

SEPTEMBER 2008

RUSSELL WINANS

BS, UNIVERSITY OF MASSACHUSETTS AMHERST

M.S.C.E., UNIVERSITY OF MASSACHUSETTS AMHERST

Directed by: Professor Sanjay R. Arwade

Wood products tend to have a very large variability resulting in over design of engineered products. A relatively new structural composite wood material, Parallel Strand Lumber (PSL) has been introduced with the expectation to reduce the inherent biological variation wood products tend to have between specimens and species. A probabilistic approach is being taken to model effective properties, strain, and strength of PSL. Biological variation of grain angle, effective properties, biological defects such as voids, strand dimensions, and constitutive species composing each PSL member were taken into account. Methods will be used to verify experimental results for the ultimate stress or maximum stress, modulus of elasticity, lengthwise variability, and stress-strain behavior of Parallel Strand Lumber made from southern yellow pine. Experimental compression data is measured from 64 A specimens with the dimensions 1.10 in x 1.10 in x 3.25 in and 162 B specimens with the dimensions

1.55 in x 1.55 in x 5.00 in. This data yields compression modulus of elasticity values of 1840 ksi with a standard deviation of 300 ksi for the A specimens and 1860 ksi with a standard deviation of 400 ksi for the B specimens. The ultimate stress at failure of the A specimens is 7.71 ksi with a standard deviation of 1.09 ksi and the ultimate stress at failure of the B specimens is 8.97 ksi with a standard deviation of 1.02 ksi. Experimental bending data is measured from 1 A specimen with the dimensions 5.25 in x 5.25 in x 192 in and 9 B specimens with the dimensions 1.55 in x 1.55 in x 96 in. These experiments yield edgewise modulus of elasticity values in bending of 1775 ksi with a standard deviation of 25 ksi for the A specimen and 1648 ksi with a standard deviation of 150 ksi for the B specimens.

TABLE OF CONTENTS

LIST OF TABLES

Table **Page**

LIST OF FIGURES

Figure **Page**

CHAPTER 1

INTRODUCTION

Parallel Strand Lumber (PSL) is a structural composite lumber that is made by bonding together long, thin, narrow strips of wood with Phenyl-Formaldehyde in a press to form a non-homogeneous composite of wood strands from one or multiple species of wood. This structural wood product is commonly used in commercial and industrial applications such as truss members, joists, columns, and beams. Parallel Strand Lumber is considered to be an economical structural material because it uses wood fiber scraps from plywood panel production which would otherwise be discarded as waste. The mixture creates a structural composite with material properties which are heterogeneous, random, and vary spatially, which differs significantly from solid wood lumber.

1.0.1 Goals

The goals of this research project are (1) determine experimentally how the cross-sectional modulus of elasticity in bending and compression as well as the ultimate compressive strength varies spatially along the length of Parallel Strand Lumber, (2) develop probability models for the material properties, mechanics of the mesostructure, and other accompanying variables, (3) develop computational models from the experimental data collected which will be used to create probabilistic characterizations of the spatially varying effective properties in both bending and compression applications, and (4) use the computational and experimental data to perform additional parameter studies such as the effect of the grain angle distribution on the modulus of elasticity.

1.1 Literature Review

The measurement and characterization of the spatially varying stiffness and strength properties in Parallel Strand Lumber is important for the continued adoption of new innovative materials for structural applications. Strength-based code design of wood structures uses a probabilistic analysis of the likelihood of failure of a structural system to determine load and resistance factors [8]. Calculation of the probability of failure relies on computational models or experiments of how the member will perform under a given load combination. These models must include probabilistic models of the material properties. This paper describes two probabilistic modeling methods for the bending modulus of elasticity and the compression modulus of elasticity and ultimate strength. Modeling of wood products tends to be very difficult because of the inherent biological variation in wood where material properties vary spatially within a member and between members.

This variability is well documented in the Wood Handbook which has a collection of experiment data on most common wood species, where typical coefficient of variations for the modulus of elasticity and failure strength are given as 20% [8]. The data given are point statistics of the effective properties of solid wood with no estimations of the spatial variation of these properties. Lam et al. [10] characterized the spatial correlation of the tensile strength of nominal 38x89 mm No. 2 Spruce-Pine Fir lumber. Results are that the tensile strength at a distance greater than 1.83 meters apart along the length can be considered statistically independent and uncorrelated. In a continuation of this work, Lam et al. [11] used the tensile strength profile results from their previous work and a moving average process to account for spatial correlation of the within member tensile strengths. Good agreement is found between model predictions and test results. These tests are performed on dimension lumber made from Spruce-Pine-Fir, which is also used in the manufacturing process of PSL which provide a useful insights for the starting point of computational models. Two signifi-

cant additions are added to ideas presented by Lam et al., which are, that the present model accounts for both variation within a member and between members, and also, the model quantitatively describes how bending tests distort the true modulus process because the bending tests effectively average the material properties between the testing span.

There are few well defined mesostructure models for Parallel Strand Lumber or other structural composites. Bejo and Lang [3] use a computer model to simulate nominal cross-sections of dimensions 75x140 mm for Parallel Strand Lumber and 45x90 mm for Laminated Veneer Lumber (LVL). Probability functions are used to randomize the geometric features (type of wood, grain angle, etc) of the composites and one thousand simulations are run. These results are compared to experimental data at different load orientations. It is found that the pure axial load orientation showed excellent agreement with test results and overall good agreement to experimental data is shown. Although the agreement of this model is excellent, the model assumes that modulus of elasticity values along the length of cross-section are constant where typically these values are only spatially correlated approximately 50 in along the cross-section. Three dimensional considerations in the current model allow for the consideration of these spatial variations of the effective properties in Parallel Strand Lumber. Hu and Wang [9] reported experimental and computational data on veneer-overlaid particleboard composites which define the mechanics model's modulus of elasticity dependency on the grain angle. Hu and Wang [9] use a similar approach as the one presented here by using orthotropic elastic equations to derive expressions for the length-wise effective modulus of elasticity, which yield exact results to one another.

Having defined a model for the mesostructure material the next goal was to identify an approach for the mechanics of Parallel Strand Lumber. Clouston and Lam [5][6][4] present modeling procedures for wood composite such as Laminated Veneer

Lumber and Parallel Strand Lumber. Stochastic-based material properties are used to develop a nonlinear finite element model where each element uses Tsai-Wu (an anisotropic failure criteria) to model strength characteristics. Key advances to modeling are the addition of length dimensions to the model which allows investigation of spatial variability.

This research begins with a description of material and mechanics models used. Next, bending and compression experimental data are presented and analyzed. Computational models then yield estimates of the modulus of elasticity, strength, and spatial variation along the length of a given cross-sectional size and member length. These computational models, once validated, are then used to present results on ensemble and other interesting statistics of the spatial variability of different member sizes.

CHAPTER 2

PROBLEM STATEMENT

2.1 Mesostructure Model Overview

The goal of the mesostructure model is to take a real section of Parallel Strand Lumber and simplify it by idealizing how the structure is composed, which is shown in Figure 2.1.

2.1.1 Assumptions and Idealizations

To effectively model the geometry of Parallel Strand Lumber several idealizations and assumptions are used. It is assumed that all of the strands, shown in Figure 2.1, are parallel to one another and perpendicular to the cross-section dimensions. This neglects the randomly oriented geometry of most strands and assumes that all of the surfaces of each strand are fully bonded to any adjacent strand. This also assumes the cross-section is free of voids which is not typical for Parallel Strand Lumber.

The Parallel Strand Lumber member cross-section is assumed to be rectangular, which is often typical for wood products. Each cross-section is composed of many strands, with the exact number depending on the size of the strands and the cross-section. These assumptions and idealizations are shown in Figure 2.1.

2.2 Material Model

2.2.1 Material Stiffness Properties

Each strand is modeled as an orthotropic material. The stress-strain relationships can be determined from twelve independent elastic constants: three modulus

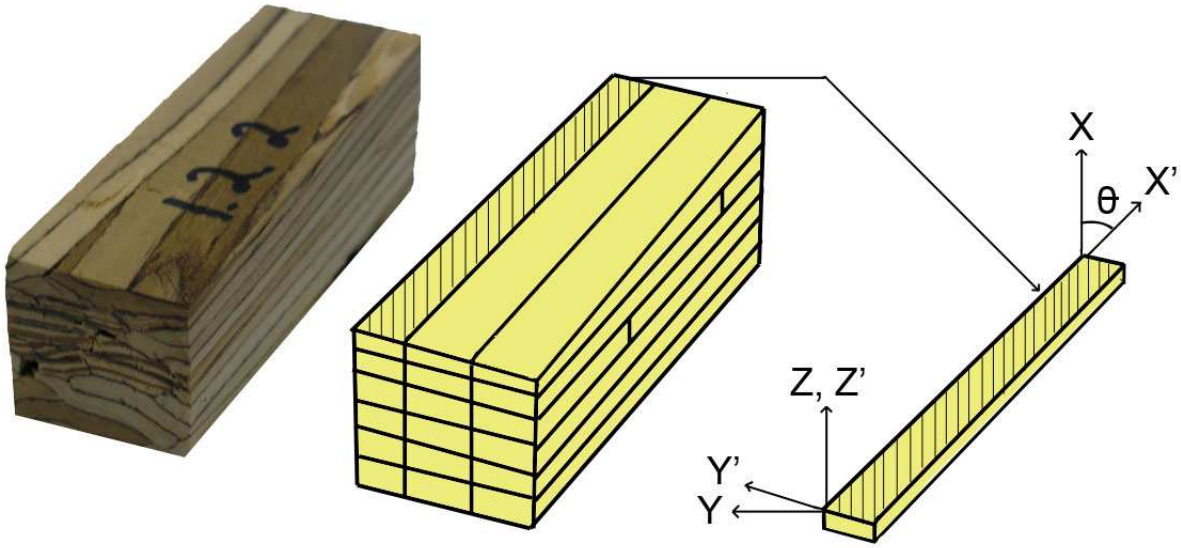

Figure 2.1. Actual and idealized Parallel Strand Lumber cross-sections.

of elasticity values E_x, E_y, E_z; three independent Possion ratios ν_{xy}, ν_{xz}, ν_{yz} (this is the result of symmetry of the modulus of elasticity and the Poisson ratio where the relationship between E_y and E_x can be expressed as $\nu_{yx}/E_y{=}\nu_{xy}/E_x$); and three shear modulus values G_{xy}, G_{xz}, G_{yz}. A standard Cartesian coordinate system is used with the three principle axis parallel to the height, width, and depth of the member. A second (x', y', z') coordinate system is used to model a strand's grain orientation.

The orthotropic stress strain relationship using the described coordinate system is defined as

$$\begin{bmatrix} \epsilon_x \\ \epsilon_y \\ \epsilon_z \\ \gamma_x \\ \gamma_y \\ \gamma_z \end{bmatrix} = \begin{bmatrix} \frac{1}{E_x} & -\frac{\nu_{yx}}{E_y} & -\frac{\nu_{zx}}{E_z} & & & \\ -\frac{\nu_{xy}}{E_x} & \frac{1}{E_y} & -\frac{\nu_{zy}}{E_z} & 0 & 0 & 0 \\ -\frac{\nu_{xz}}{E_x} & -\frac{\nu_{yz}}{E_y} & \frac{1}{E_z} & 0 & 0 & 0 \\ 0 & 0 & 0 & \frac{1}{G_{xy}} & 0 & 0 \\ 0 & 0 & 0 & 0 & \frac{1}{G_{xz}} & 0 \\ 0 & 0 & 0 & 0 & 0 & \frac{1}{G_{yz}} \end{bmatrix} \begin{bmatrix} \sigma_x \\ \sigma_y \\ \sigma_z \\ \tau_x \\ \tau_y \\ \tau_z \end{bmatrix}. \tag{2.1}$$

2.2.2 Material Strength Properties

For wood materials, the failure criteria typically used to describe a material's failure envelope are Tsai-Hill or Tsai-Wu [6]. The Tsai-Hill failure criterion for a particular stress state is described as

$$((G+H)(\sigma_i\cos(\theta)^2)^2 + (F+H)(\sigma_i\sin(\theta)^2)^2 - 2H\sigma_i\cos(\theta)^2\sigma_i\sin(\theta)^2 + 2N(\sigma_i\cos(\theta)\sigma_i\sin(\theta))^2 < 1 \tag{2.2}$$

with

$$F = \frac{1}{2}(-\frac{1}{F_x^2} + \frac{1}{F_y^2} + \frac{1}{F_z^2}) \tag{2.3}$$

$$G = \frac{1}{2}(\frac{1}{F_x^2} - \frac{1}{F_y^2} + \frac{1}{F_z^2}) \tag{2.4}$$

$$H = \frac{1}{2}(\frac{1}{F_x^2} + \frac{1}{F_y^2} - \frac{1}{F_z^2}) \tag{2.5}$$

$$L = \frac{1}{2S_{yz}} \tag{2.6}$$

$$M = \frac{1}{2S_{xz}} \tag{2.7}$$

$$N = \frac{1}{2S_{xy}} \tag{2.8}$$

$$\theta = \text{strand's grain angle} \tag{2.9}$$

$$\sigma_i = \text{uni-axial stress in strand i} \tag{2.10}$$

In the above expression the maximum allowable uni-axial stress in one of the principle directions are noted as F_x, F_y, F_z. The maximum allowable shearing stress in two of the principle planes are denoted as S_{xy}, S_{yz}, and S_{xz}.

2.3 Deterministic and Random Parameters

2.3.1 Deterministic Parameters

For each model the cross-sectional geometry of each strand is assumed to be deterministic according to experimental measurements on actual cross-sections of Parallel Strand Lumber. The width w_i is determined to be 0.2 in and the depth d_i is determined to be 0.5 in.

2.3.2 Random Parameters

Each strand has associated properties that are considered to be random variables. These associated properties are the strand's grain angle θ_i, nine independent elastic constants $E_{x,i}$, $E_{y,i}$, $E_{z,i}$, $\nu_{xy,i}$, $\nu_{xz,i}$, $\nu_{yz,i}$, $G_{xy,i}$, $G_{xz,i}$, $G_{yz,i}$, six independent plastic constants F_x, F_y, F_z, S_{xy}, S_{yz}, S_{xz} and length L_i. All of the random variables are assumed to be independent, which is not typical. Length-wise variability of the modulus of elasticity and strength within a strand is not considered.

The grain angle of each strand is assumed to be a random variable with the probability mass function shown in Figure 2.2 (Clouston, 2006). Each grain angle is taken as a random variable with distinct values $\theta(k)$ with probabilities $F(\theta^{(k)})$:=$P(X < \theta_i)$=$\sum_{i:\theta_i<\theta} p(\theta_i)$. For two adjacent values $\theta_{j-1} < \theta_j$ the probability is equal to $P(\theta_j)$=$F(\theta_j)$-$F(\theta_{j-1})$. The generalized grain angle probability mass function has the form $f_Y(\theta)$=$\sum_i P(Y = \theta^{(i)}\delta(\theta - \theta^{(i)})$.

The simulation algorithm set $\theta = \theta_k$, where $k = \text{argmin}_k(\sum_{i=1}^{k} p(\theta_i < U))$, where U is a uniform random variable on the interval [0,1]. This yields the corresponding grain angle for each strand from the generalized probability mass function. Each grain angle was then considered to have the following property: $P(\theta = \theta) = 0.5$ and $P(\theta = -\theta) = 0.5$ to make the probability mass function symmetric about θ=0.

The material elastic and strength constants of each strand are assumed to have an expected value and coefficient of variation (COV) chosen to agree with experimental

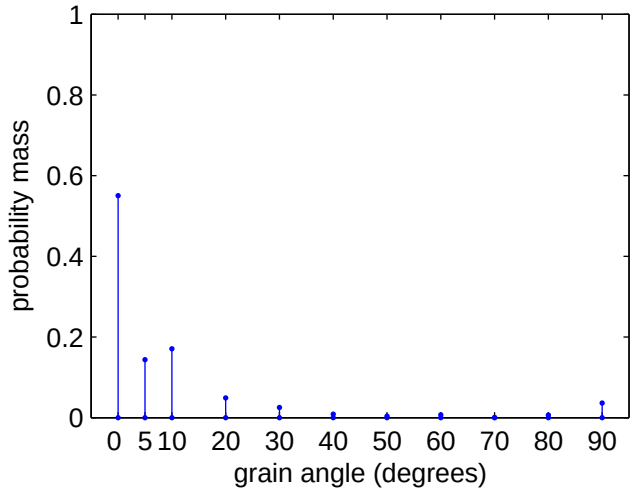

Figure 2.2. Grain angle probability mass distribution.

tests (Wood Handbook, 1994) for each type of wood species modeled. Using the x-axis modulus of elasticity as an example, the elastic constants of each strand are assumed to be Gaussian random variables with mean equal to the expected value of the modulus of elasticity, and the standard deviation given by $\sigma = COV \times (E[E_x])$. This yields an expression for each of the elastic constants, where the modulus of elasticity about the x-axis, is $E_x = E[E_x] + W$, where $E[\bullet]$ is the expectation operator and $W \sim N(0, \sigma^2)$. The material constants for the computational model are $E_x =$ 1886 ksi, $E_y = 119.3$ ksi, $G_{xy} = 128.4$ ksi, $\nu_{xy} = 0.022$, $F_x = 8.31$ ksi, $F_y = 1.74$ ksi, and $S_{xy} = 1.59$ ksi.

The strand length is assumed to follow a beta distribution with parameters $\beta = 2$ and $\alpha = 5$ on the interval from [2,8] ft and is given by $L_i = 2 + 6\beta$, where $\beta \sim \beta(5, 2)$. The choice of this distribution is made because the length of most strands tend to be approximately 8 feet, and fewer strands are of shorter length, which is due to the manufacturing process. The expected value of the length of a strand is , $E[L_i] = 2 + 6\frac{\alpha}{\alpha+\beta}$.

2.4 Specimen Types and Loads

2.4.1 Compression Test Setup

The compression test setup is staged to simulate a specimen which is fixed at one end and with an applied displacement at the other. The cross-sectional dimensions d_s and w_s and the length L_s are chosen in such a way as to ensure crushing failure rather than buckling of the column under the given load P. A schematic of the compression setup for the computational models can be seen in Figure 2.3 and the actual experimental setup in Figure 2.4.

2.4.2 Bending Test Setup

The bending test setup is staged in such a way as to permit observation of the bending modulus as a random process at a series of defined points along the length of a specimen. To measure the elastic modulus of the Parallel Strand Lumber specimen bending tests were performed whose material models and solution methods are outlined in Chapter 3. Each bending specimen has a total length denoted by L_T, the span between pin-roller support location is L_{sup}, and the spacing of tests along the length of the specimen is L_s. The load P applied at time step d_t is a user defined constant. A schematic of the computational test setup can be seen in Figure 2.5 with the actual test setup in Figure 2.6.

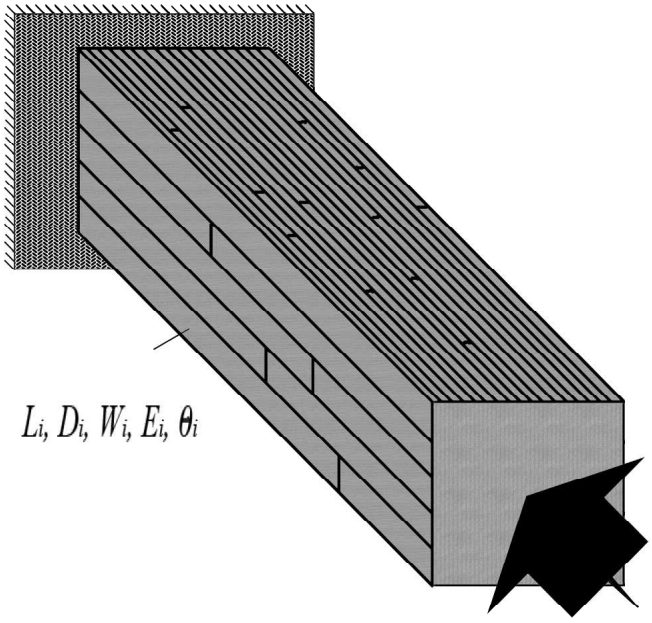

Figure 2.3. Compression test setup schematic of an idealized cross-section with length variation.

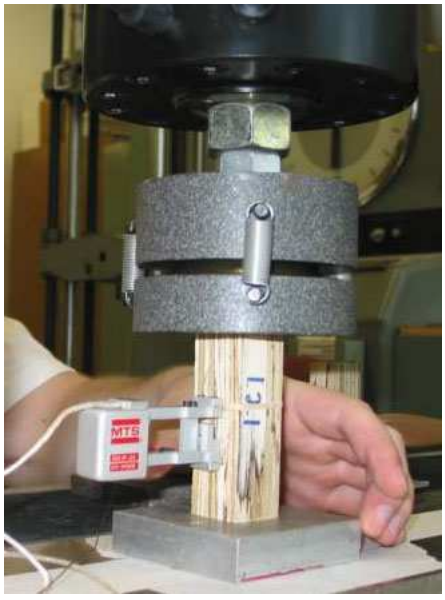

Figure 2.4. Experimental compression test setup of a 1.10 in x 1.10 in x 3.25 in sample.

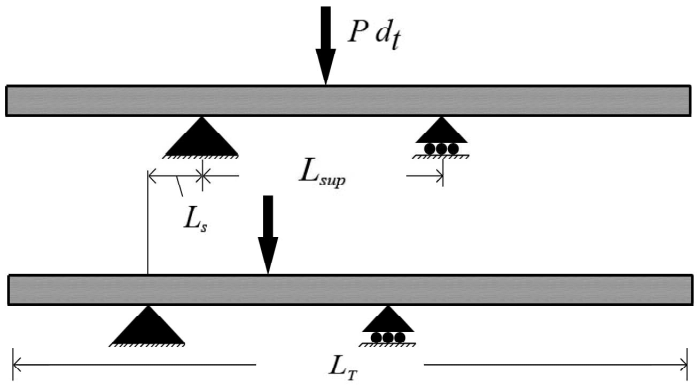

Figure 2.5. Bending test setup schematic showing the passage of a test specimen through two support locations.

Figure 2.6. Bending test setup of a 5.25 in x 5.25 in x 16 ft experimental sample.

CHAPTER 3

COMPUTATIONAL MODELS

3.1 Overview

Computational models are used to provide the flexibility needed to do parameter studies without physical experiments. These models will be validated from experimental data and then used to observe parameters such as estimations of the ensemble correlation length of the modulus of elasticity or ultimate stress in Parallel Strand Lumber.

3.2 Stiffness Model

The goals of the stiffness model are to use an orthotropic mechanical model and apply stress-strain transformations on the constitutive matrix to derive a relationship between the applied uni-axial stress and strain in a cross-section of parallel strands. This will then yield an estimate of the modulus of elasticity along the longitudinal x'-axis.

3.2.1 Assumptions

Due to a cross-section of Parallel Strand Lumber being composed of many strands which have varying grain angles a displacement controlled model is used. This uniform displacement results in a constant strain approach which is appropriate because of the assumption of perfect bonds between strands. Also, it is assumed that because all strands are fully bonded to one another they act as a single body.

3.2.2 Effective Modulus Derivation

The effective modulus of elasticity for a strand is defined as the material stiffness with respect to the longitudinal x'-axis, which is defined as $E_{x',strand} = \sigma_{x\prime}/\epsilon_{x\prime}$ with the coordinate system defined in Figure 3.1.

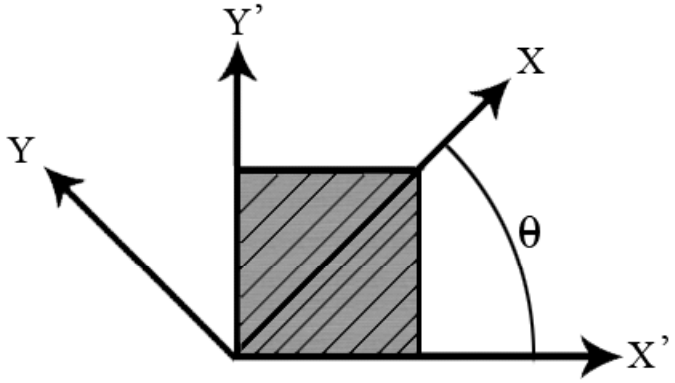

Figure 3.1. Grain angle coordinate system.

A orthotropic stress strain relationship is used to formulate an expression for the effective modulus of elasticity for each strand.

$$\begin{bmatrix} \epsilon_x \\ \epsilon_y \\ \epsilon_z \\ \gamma_x \\ \gamma_y \\ \gamma_z \end{bmatrix} = \begin{bmatrix} \frac{1}{E_x} & -\frac{\nu_{yx}}{E_y} & -\frac{\nu_{zx}}{E_z} & & & \\ -\frac{\nu_{xy}}{E_x} & \frac{1}{E_y} & -\frac{\nu_{zy}}{E_z} & 0 & 0 & 0 \\ -\frac{\nu_{xz}}{E_x} & -\frac{\nu_{yz}}{E_y} & \frac{1}{E_z} & 0 & 0 & 0 \\ 0 & 0 & 0 & \frac{1}{G_{xy}} & 0 & 0 \\ 0 & 0 & 0 & 0 & \frac{1}{G_{xz}} & 0 \\ 0 & 0 & 0 & 0 & 0 & \frac{1}{G_{yz}} \end{bmatrix} \begin{bmatrix} \sigma_x \\ \sigma_y \\ \sigma_z \\ \tau_x \\ \tau_y \\ \tau_z \end{bmatrix}. \tag{3.1}$$

Stress and strain transformations are

$$\begin{bmatrix} \sigma_{x'} \\ \sigma_{y'} \\ \tau_{x'y'} \end{bmatrix} = \begin{bmatrix} \cos^2\theta & \sin^2\theta & 2\sin\theta\cos\theta \\ \sin^2\theta & \cos^2\theta & 2\sin\theta\cos\theta \\ -\sin\theta\cos\theta & \sin\theta\cos\theta & \cos^2\theta - \sin^2\theta \end{bmatrix} \begin{bmatrix} \sigma_x \\ \sigma_y \\ \tau_{xy} \end{bmatrix} \tag{3.2}$$

$$\begin{bmatrix} \epsilon_{x'} \\ \epsilon_{y'} \\ \frac{1}{2}\gamma_{x'y'} \end{bmatrix} = \begin{bmatrix} \cos^2\theta & \sin^2\theta & 2\sin\theta\cos\theta \\ \sin^2\theta & \cos^2\theta & 2\sin\theta\cos\theta \\ -\sin\theta\cos\theta & \sin\theta\cos\theta & \cos^2\theta - \sin^2\theta \end{bmatrix} \begin{bmatrix} \sigma_x \\ \epsilon_y \\ \frac{1}{2}\gamma_{x'y'} \end{bmatrix}. \tag{3.3}$$

Imposing uni-axial stress to the stress transformation matrix yields

$$\begin{bmatrix} \sigma_0 \\ 0 \\ 0 \end{bmatrix} = \begin{bmatrix} \cos^2\theta & \sin^2\theta & 2\sin\theta\cos\theta \\ \sin^2\theta & \cos^2\theta & 2\sin\theta\cos\theta \\ -\sin\theta\cos\theta & \sin\theta\cos\theta & \cos^2\theta - \sin^2\theta \end{bmatrix} \begin{bmatrix} \sigma_x \\ \sigma_y \\ \tau_{xy} \end{bmatrix}. \tag{3.4}$$

Next, stresses in the strand coordinate system are solved for in terms of the applied stress σ_0

$$\sigma_x = \frac{\sigma_0(1 + \cos2\theta)}{2} \tag{3.5}$$

$$\sigma_y = -\frac{\sigma_0(-1 + \cos2\theta)}{2} \tag{3.6}$$

$$\tau_{xy} = \frac{\sigma_0(\sin2\theta)}{2}. \tag{3.7}$$

From the transformed strain matrix the following relationships are taken and trigonometric substitutions performed on ϵ_x, ϵ_y, and γ_{xy} from equation 3.1 to yield an expression for the strain in the strand coordinate system.

$$\epsilon_{x'} = \epsilon_x\cos^2\theta + \epsilon_y\sin^2\theta + \gamma_{xy}\sin\theta\cos\theta. \tag{3.8}$$

Solving for $E_{x',strand}$ and $\sigma_{x'}$ assuming $\sigma_{x'} = \sigma_0$ with all other stress states equal to zero yields an equation for the effective modulus of elasticity of a strand

$$E_{x',strand} = \frac{\sigma_{x'}}{\epsilon_{x'}}. \tag{3.9}$$

$$E_{x'strand} = \frac{4E_xC}{C + 2C\cos2\theta - 2D\nu_{yx} + D\cos2\theta + C\cos^2\theta + 2D\cos^22\theta\nu_{yx} + D\cos^2\theta + E_xE_y - CE_x\cos^22\theta} \tag{3.10}$$

with

$$C = E_yG_{xy}$$

$$D = E_xG_{xy}.$$

3.2.3 Linear Mixture Model Overview

Due to Parallel Strand Lumber being a composite, an average or effective modulus of elasticity of the cross-section $E_{x',section}$ must be calculated to determine the global behavior of the material. To calculate this, it is assumed that the strain in each strand is equal to the applied strain, $\epsilon_i = \epsilon_0$. The stress in each strand $\sigma_i = \epsilon_0 E_{x',i}$. The force in each strand is then calculated as $P_i = \sigma_i A_i$. The total force applied to the cross-section is $P = \sum_i P_i$. The average stress in the cross-section is $\sigma_0 = P/\sum_i A_i$. The effective modulus of the cross-section or average of the strand moduli is then calculated as $E_{x',section} = \sigma_0/\epsilon_0$.

3.3 Strength Model

The goals of the strength model are to use an appropriate failure criteria in conjunction with the stiffness model described in the previous sections to yield estimates of the stress-strain relationship in the post elastic region, and of the ultimate stress at failure of the cross-section.

3.3.1 Assumptions

The strength model assumes that there is constant strain throughout the cross-section. Under the applied uni-axial stress it is assumed that $\sigma_z = \tau_{xz} = \tau_{yz} = 0$. Wood products typically fail in two ways depending on the loading. In compression the material is assumed to fail in a ductile way and in tension it is assumed that the material fails in a brittle manner. Therefore, in compression the material's behavior post yield is assumed to be elastic-perfectly plastic and in tension the material's behavior is brittle having no additional load capacity upon reaching the failure surface.

3.3.2 Strength Model

By applying a strain ϵ_0 the stress in strand i can be calculated as $\sigma_i = \epsilon_0 E_{x',i}$. Using stress transformations in the three principal directions, the Tsai-Hill failure criterion can be expressed as the following given a strand's grain angle, its material properties, and the known uni-axial stress in compression or tension σ_i

$$((G+H)(\sigma_i \cos(\theta)^2)^2 + (F+H)(\sigma_i \sin(\theta)^2)^2 - 2H\sigma_i \cos(\theta)^2 \sigma_i \sin(\theta)^2 + 2N(\sigma_i \cos(\theta)\sigma_i \sin(\theta))^2 < 1 \qquad (3.11)$$

The total stress within the cross-section is σ_0 which is calculated as $\sigma_0 = \frac{\sum_i P_i}{A_{total}}$ where $P_i = \sigma_i A_i$ with the strength found using the parallel system model.

3.4 Finite Element Model

3.4.1 Overview of Finite Element Model

The finite element modeling program that is used for analysis is Adina v8.3.3 [1]. The total cross-sectional dimensions of each model are the depth d_0, width w_0, and length L_0. Each strand is assigned dimensions which are d_i, w_i, and L_i that are based on user input. The meshing subdivision length in the principal x', y', and z' directions

for each model are determined from convergence studies. The convergence studies will be shown in more detail in chapter 7 which has the results of the finite element analysis. The elements used are rectangular three-dimensional 27 node quadratic block elements.

3.4.2 Compression Finite Element Model

The compression and tension models assume that one end is fixed in the x' direction located where $x' = 0$. Line constraints in the z' and y' directions prevent translation and are located where $y' = \frac{1}{2}d_0$, $z = \frac{1}{2}w_0$, and $x' = 0$. A uniform time varying displacement d_t is applied to the $y' - z'$ plane where $x' = L_0$.

The effective modulus of the cross-section is calculated as $E_{x',section,t} = \frac{\sigma_{x',t}}{\epsilon_{x',t}}$, where the subscript t denotes a time step in the analysis. The strain is calculated as $\epsilon_{x',t} = \frac{L_0 - d_t}{L_0}$ and $\sigma_{x',t}$ is calculated as $\sigma_{x',t} = \frac{\sum_i R_{i,t}}{A_{total}}$ where $R_{i,t}$ are the reaction forces on the $y' - z$ plane where $x' = L_0$ at time step t. An example of a compression finite element model is shown in Figure 3.2.

3.4.3 Bending Finite Element Model

The bending model assumes the beam setup is that of a simply supported beam with a midpoint load. The fixities to provide a simply supported condition are applied at $x' = L_0$ and $x' = 0$ along the z-axis about the line $y' = \frac{1}{2}d_0$. The fixity of these nodes along this line are fixed and prevent translation the x' and y'-directions. An example of a bending finite element model is shown in Figure 3.3.

3.5 Finite Difference Model

A finite difference solution is used to numerically calculate the mid-span deflection of a simply supported beam with a midpoint load and variable modulus of elasticity. The displacement is a function of the effective modulus of elasticity $E_{x',j}$ where there are n nodes on the interval $[a, b]$ with $j = 0, 1, ..., n - 1$, the length

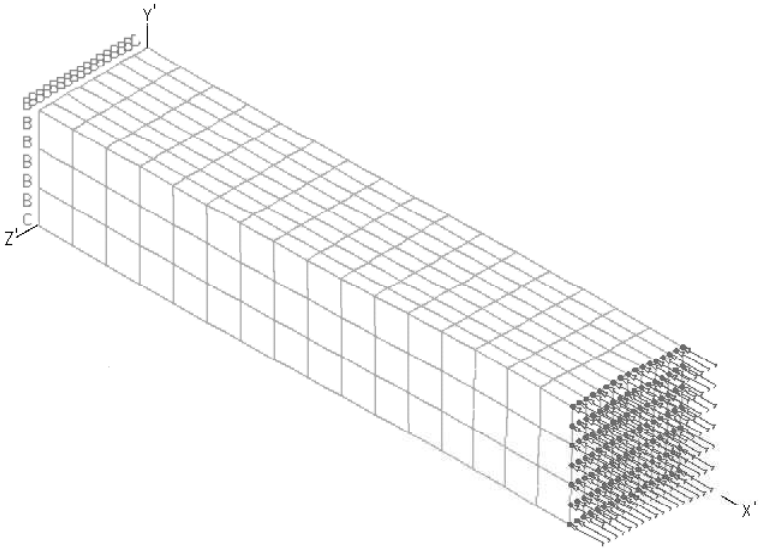

Figure 3.2. An example of a compression finite element model. Boundary conditions and displacement locations are shown at the ends of the model.

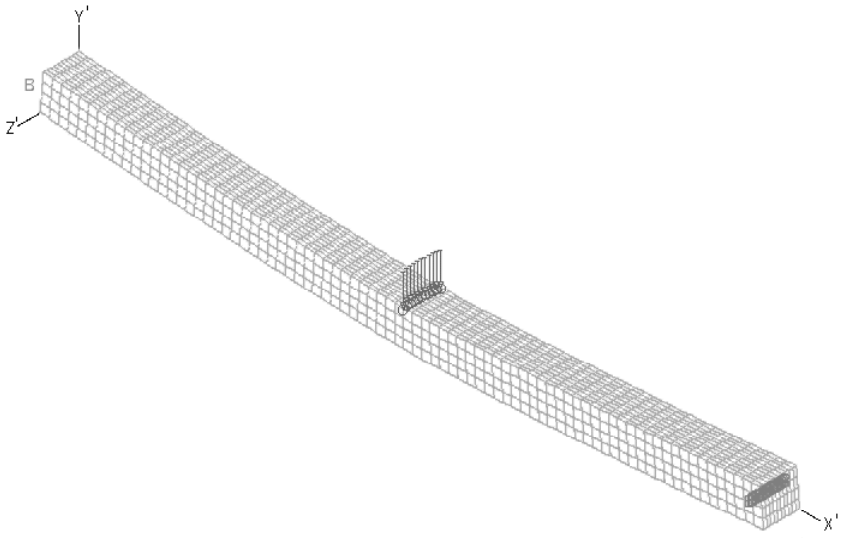

Figure 3.3. An example of a bending finite element model. Boundary conditions are shown at the ends of the model with a applied load in the center of the beam.

of the span L_{spanab}, which is equal to the distance between the support locations a and b in the x'-direction, the cross-sectional dimensions w_0 and d_0, and the load P ($\delta = f(E_{x',j}, w_0, d_0, L_{spanab}, P)$).

A second order finite difference on the beam equation is used, which is

$$E(x)Iv'' = M(x) \tag{3.12}$$

CHAPTER 4

EXPERIMENTS

4.1 Outline and Goals

Compression and Bending tests are performed on Parallel Strand Lumber made from southern yellow pine. These experimental tests are used to investigate the spatial variation of the modulus of elasticity and the ultimate stress in compression. Uniaxial compression tests are performed on two sample sizes 1.55 in x 1.55 in x 5 in and 1.10 in x 1.10 in x 3.25 in specimens which yields estimations of the modulus of elasticity and ultimate stress. Three point bending experiments were performed on two specimen sizes 5.25 in x 5.25 in x 16 ft and 1.55 in x 1.55 in x 8 ft which yielded estimations of the bending modulus of elasticity. The goals of these experiments were to (1) gather more data on the effective properties of Parallel Strand Lumber, (2) gather estimates of the spatial variability of the effective properties, and (3) use the data to validate computational models.

4.2 Compression Tests

4.2.1 Overview of Compression Tests

Experimental tests were used to investigate the spatial variation of the compression modulus of elasticity and ultimate stress of Parallel Strand Lumber. These experimental tests were performed on a two members of PSL made from southern yellow pine where the first was 2.66 in x 5.25 in x 27 in in dimension which was machined into eight members with the dimensions of 1.10 in x 1.10 in x 27 in. These were then machined again into 64 1.10 in x 1.10 in x 3.25 in compression specimens,

a schematic is shown in figure 4.1. The second round of compression testing was performed on samples from a member of dimensions 5.25 in x 5.25 in x 16 ft. This member was machined into nine 1.55 in x 1.55 in x 8 ft specimens then machined again into 162 1.55 in x 1.55 in x 5 in compression specimens, a schematic is shown in figure 4.2. These sizes are chosen in accordance to ASTM standards [2]. The experimental testing consisted of a series of compression tests to failure, which observed the modulus of elasticity and ultimate stress as a random process along the length of the member. From these experiments the mean, variance, and lengthwise auto-correlation of the compression modulus of elasticity and ultimate stress could be estimated. A formulation for the scaled auto-covariance function used is defined as

$$\rho(i,j) = \frac{(\hat{Y}_{eff,i} - E[\hat{Y}_{eff,i}])(\hat{Y}_{eff,i+j} - E[\hat{Y}_{eff,i+j}])}{\sigma^2_{\hat{Y}_{eff}}} \tag{4.1}$$

where $E[\bullet]$ is the expectation operator, and σ is the standard deviation of the process $\hat{Y}_{eff}$ in a single sample or an ensemble of samples. This formulation for the auto-covariance assumes there are n sample observation locations located along the length of a member for which $i = 1, ..., n$. Assuming that the sample spacings are evenly distributed along the length there will be j available locations to estimate the correlation with j defined as the number of samples away from i where j varies from $i, i+1, ..., i+n-1$ with $i + j < n$.

The measurements obtained represent a piece-wise smoothed version of the true modulus and strength fields due to averaging of material properties. The motivation of these tests was to gain statistics of mean, variance, and correlation length which will be used to validate computational models and case studies.

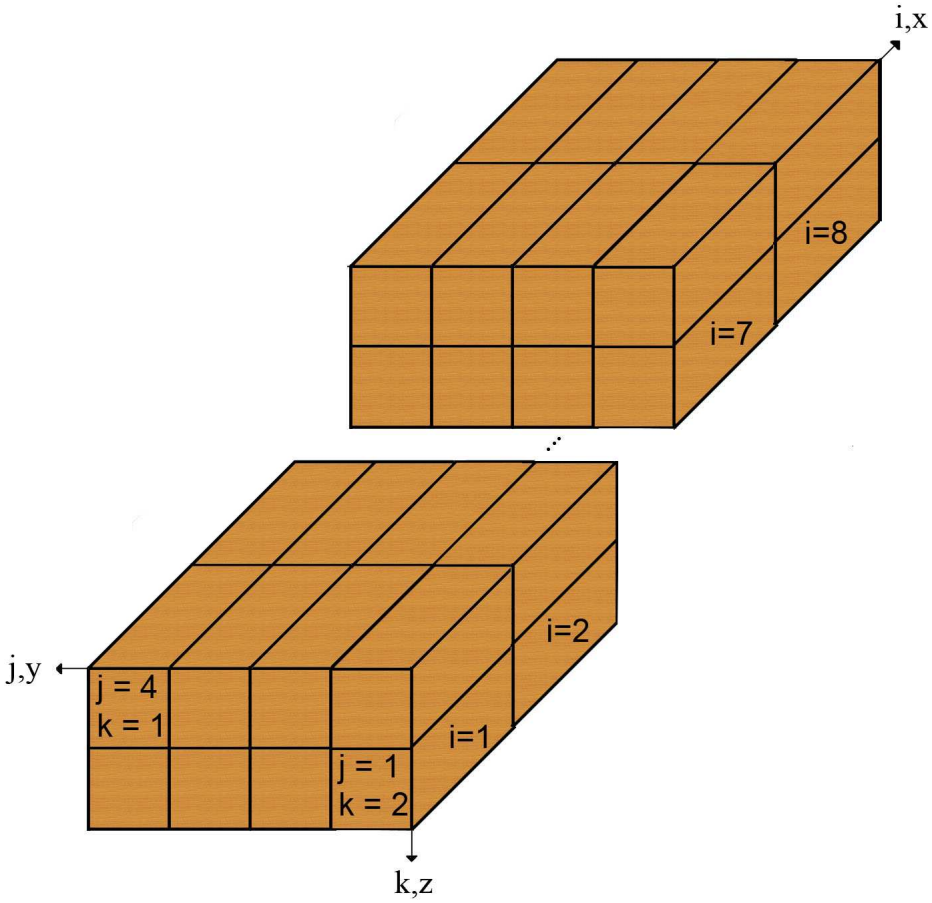

Figure 4.1. Schematic for 64 specimens in group A.

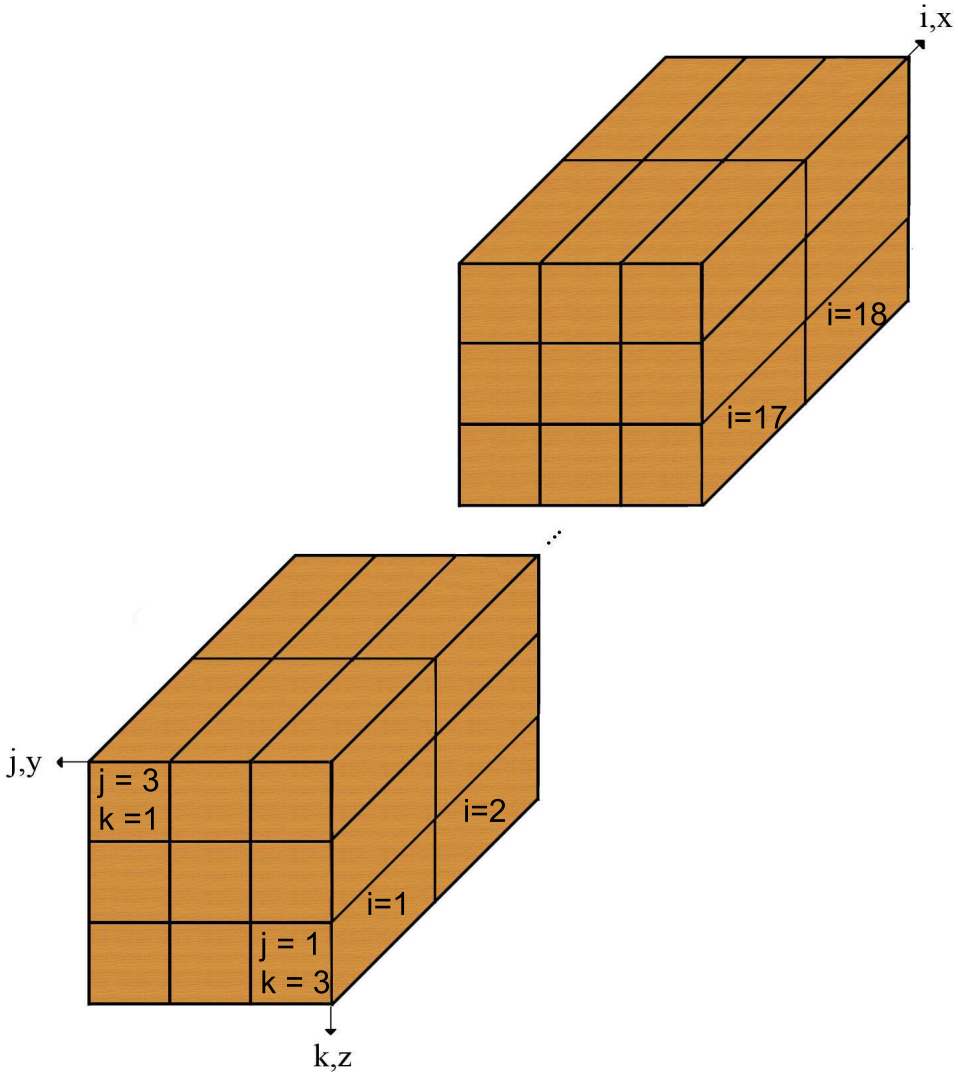

Figure 4.2. Schematic for 162 specimens in group B.

4.2.2 Results of Compression Tests Round 1

To measure the compression elastic modulus of the Parallel Strand Lumber specimens compression tests were performed with geometric limits defined by ASTM standard [2] to ensure crushing dominated behavior. Two specimen groups were used to capture size effects of the averaging of strands in a given cross-section. Where specimen group A consists of samples with a 1.10 in x 1.10 in cross-section and group B have a cross-section size of 1.55 in x 1.55 in. Specimens A1 through A8 are from a section of lumber used in a previous bending to failure study and are made from southern yellow pine. Specimens B1 through B9 are from a section of yellow pine which were used previously in nondestructive bending tests up to 10% of their maximum capacity. A series of tests described below were performed on eight specimens A1 through A8 and nine specimens B1 through B9. Compression tests were performed on 64 specimens from group A and 162 specimens from group B to observe the modulus of elasticity and ultimate stress as a random process along the length. Each compression specimen had a total section length denoted by L_T, width w, depth d, and height h. Table 4.1 gives the numerical values of each of these parameters below for specimen groups A and B.

Table 4.1. Compression test geometry and parameters.

Group	w (in)	d (in)	h (in)	L_T (in)
A	1.10	1.10	3.25	27
B	1.55	1.55	5.00	96

Experimental tests were conducted in the Holdsworth Hall wood technology lab at the University of Massachusetts, Amherst using a screw driven MTS 30,000 lbs testing device operating in displacement control with a swivel head to ensure even load distribution across the cross-section. These tests were conducted under displacement control at an applied load rate of 0.01 in/min. This rate was used to ensure completion

of each test between 5 and 15 minutes. Tests were performed past their ultimate stress peaks until the load was reduced to approximately 80-90% of the peak load to ensure there would be no damage to the measuring equipment. The strain in each strand was measured from a cross-head displacement reading and an extensometer attached to the edgewise side of the specimen. The extensometer was used to estimate a more accurate stress-strain curve in the linear-elastic regime for each specimen.

The ultimate stress was assumed to be the peak stress in the stress-strain curve. The modulus of elasticity was estimated from the linear-elastic range of the stress-strain curve as the slope of the best fit line that portion of the graph. It should be noted that for many of the samples there is significant seating of the load head into the member so the region in which the slope is calculated is taken by eye from the most linear portion of the stress-strain curve and solved in Matlab. The stress-strain curves for both Groups A and B are shown below in Figures 4.3 and 4.4.

It should be noted that at approximately 70% of the pre-peak stress for several of the specimens the strains look to be reversing, this is due to micro buckling and damage on the outer strands which causes the readings of the extensometer attached to the side of the compression specimen to yield false readings. The extensometer is only accurate in the linear-elastic region when there is no damage to any of the strands or the structure of the compression specimen. Damage was observed in three samples from Group A and eight samples from Group B in early stages of the compression tests. Modulus of elasticity data could not be readily obtained from these specimens due to micro-buckling disrupting the extensometer readings. These samples were still tested beyond their peak loads.

The overall behavior of the compression specimens are linear-elastic with little to no strain hardening in the non linear regime which is typical for most wood materials. For some of the specimens micro buckling of individual strands was seen as

well as delamination and cracking within the specimen. Most failures occurred by delamination of several strands after significant crushing was observed.

The results of the testing are shown in Table 4.2. It is shown from the data that the ultimate stress mean of group A is 7.71 ksi which is slightly lower than group B's mean which is 8.97 ksi. The lower mean stress in the A samples is likely due to a size effect. This size effect is a results of the voids in a cross-section, which on a large scale have little effect on the inherent properties, but for small cross-sections, such as the ones tested in this research, the small voids affect the small specimens more, which lowers the ultimate stress at failure.

The ensemble coefficient of variation of the ultimate stress for group A is 14% which is slightly higher than group B, which is 11%. (For solid dimension lumber the coefficient of variation for compression parallel to grain is 18% [8].) The difference in A and B's could be attributed to the difference in overall number of strands in each cross-section which is greater in group B. This larger number of strands causes more averaging of material properties to be observed. For the smaller cross-section there are fewer strands which leads to less averaging of material properties within a given cross-section.

Groups A and B had very similar mean values for the modulus of elasticity which were 1840 ksi and 1860 ksi, respectively. For the modulus values the coefficient of variation was less for the smaller specimens at a value of 300 ksi, compared to a value of 400 ksi for the larger samples. This difference cannot be explained directly to any material properties, but may be assumed to be experimental error or the difference in the base woods used to manufacture each of the specimens because they were obtained at different periods in time. Several modulus of elasticity readings could not be obtained from three samples in group A and eight samples in group B because of premature buckling and delamination of single strands caused errors in reading the true strain. These tests were brought to peak loads, but no modulus of elasticity data

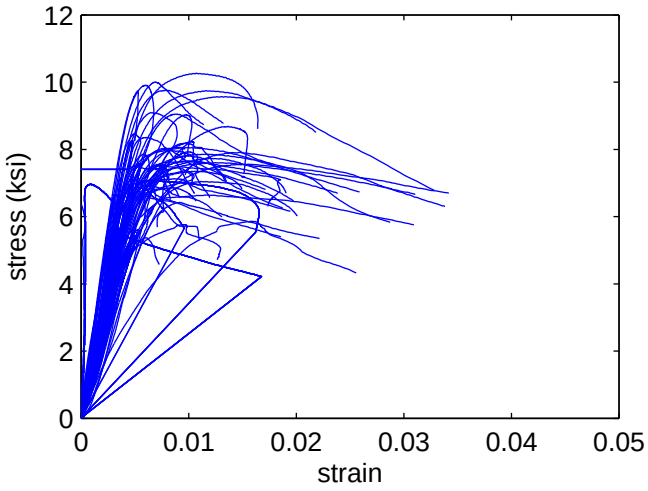

Figure 4.3. Stress-strain curves for 64 specimens in group A.

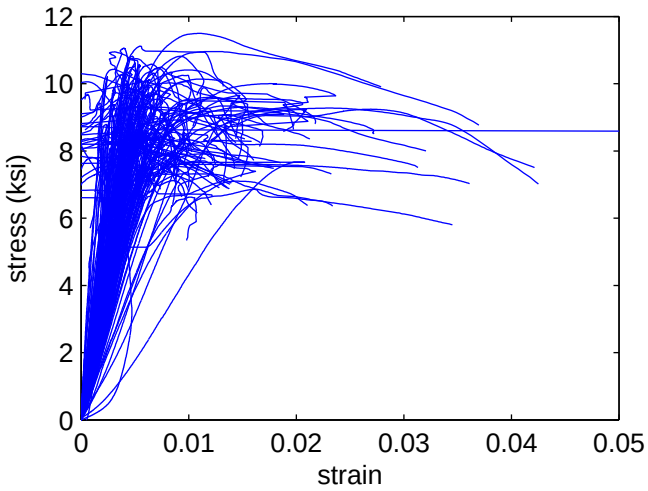

Figure 4.4. Stress-strain curves for 162 specimens in group B.

could be estimated. Overall, the modulus of elasticity readings in the compression specimens do not seem to be valid estimations of the compression modulus of elasticity and its variation.

A comparison to other work on Southern Pine Parallel Strand Lumber report members having an ultimate compression strength of 7.9 ksi for 1.5 in x 1.5 in x 7.0 in samples with a coefficient of variation of 0.87 ksi (COV 11.1%) [12]. These values are comparable with both rounds of compression tests having means of 7.71 ksi and 8.97 ksi. The variation from the means are also similar where group A has a coefficient of variation of 14% and group B has a coefficient of variation of 11%.

In the literature no compression modulus of elasticity could be obtained, but Lee and Liu report that the edgewise and flat-wise bending modulus of elasticity for Southern Pine PSL, which are 1720 and 1710 ksi, respectively [12]. The coefficient of variation of the edgewise modulus of elasticity is 12.2% and the flat-wise having a coefficient of variation of 24.0%. Group A and B samples were found to have a slightly higher modulus of elasticity of 1840 ksi for Group A and 1860 ksi for Group B. It is typical that the compression modulus of elasticity for most wood species is greater in comparison to their respective bending modulus of elasticity. The coefficient of variation for the Group A and Group B is 16% and 22%, respectively. These values are similar to the coefficient of variation published [8]. By using published data to compare to experimental results, the work presented in this chapter can be validated. From this validation a more detailed investigation of the modulus of elasticity and ultimate stress is performed to see how these material properties vary spatially within a member.

It should be observed that the modulus of elasticity and ultimate stress processes appear to be weakly stationary about their respective mean value, while in dimension lumber these processes tend to behave as a non-stationary process [10][11]. Where a weakly stationary process is a process where the mean and variation do not change

Table 4.2. Compression test results.

	ultimate stress		compression modulus	
Group	mean (ksi)	std. dev. (ksi)	mean (ksi)	std. dev. (ksi)
A1	7.48	0.44	2000	328
A2	6.48	0.95	1790	380
A3	7.81	0.37	1780	130
A4	7.44	0.42	1780	424
A5	8.36	0.49	1680	160
A6	9.76	0.32	1530	333
A7	7.46	0.48	2270	251
A8	6.88	0.90	1840	414
B1	10.3	0.55	2080	370
B2	10.1	0.61	1980	376
B3	8.77	0.68	1720	422
B4	9.87	0.48	1970	530
B5	9.16	0.58	1760	360
B6	8.17	0.57	1800	430
B7	8.62	0.51	1730	330
B8	8.31	0.34	2030	400
B9	7.46	0.50	1690	360
A ensemble	7.71	1.09	1840	300
B ensemble	8.97	1.02	1860	400
A means	–	1.01	–	–
A std. devs.	0.55	–	220	–
B means	–	0.96	–	–
B std. devs.	0.53	–	151	–

with respect to position. This is shown in Figures 4.5 and 4.6 for Groups A and B for the ultimates stress and in Figures 4.7 and 4.8 for modulus of elasticity.

To characterize the spatial variation of the compression modulus of elasticity and ultimate stress a formulation for the scaled auto-covariance function is used, it is defined as

$$\rho(i,j) = \frac{(\hat{Y}_{eff,i} - E[\hat{Y}_{eff,i}])(\hat{Y}_{eff,i+j} - E[\hat{Y}_{eff,i+j}])}{\sigma^2_{\hat{Y}_{eff}}} \tag{4.2}$$

where $E[\bullet]$ is the expectation operator, and σ is the standard deviation of the process $\hat{Y}_{eff}$ in a single sample or an ensemble of samples. This formulation for the auto-covariance assumes there are n sample observation locations located along the length of a member for which $i = 1, ..., n$. Assuming that the sample spacings are evenly distributed along the length there will be j available locations to estimate the correlation with j defined as the number of samples away from i where j varies from $i, i+1, ..., i+n-1$ with $i + j < n$.

The scaled auto-covariance function of a weakly stationary process can be estimated using either the ensemble estimates or a collection of single sample estimates of a process. If the samples are long enough these two estimates of the auto-covariance will converge to the same values. If the samples are not of significant length or if the process is not ergodic, the sample estimations will be substantially different from the ensemble estimate and exact scaled auto-covariance.

Figure 4.9 and Figure 4.10 below shows the sample estimates of the scaled auto-covariance correlation length for the ultimate stress for specimen groups A and B with the correlation length L_c of a specimen is defined as

$$L_c = argmax\rho(i,j) : |\rho(i,j)| > exp(-1). \tag{4.3}$$

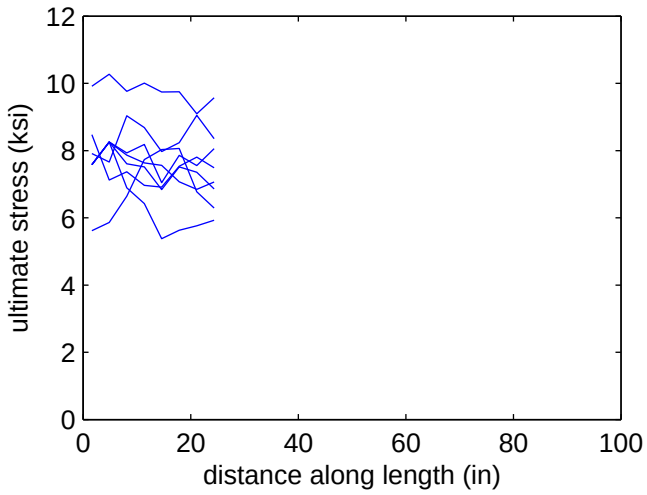

Figure 4.5. Observations of the ultimate stress acting as a random process along the length of Group A.

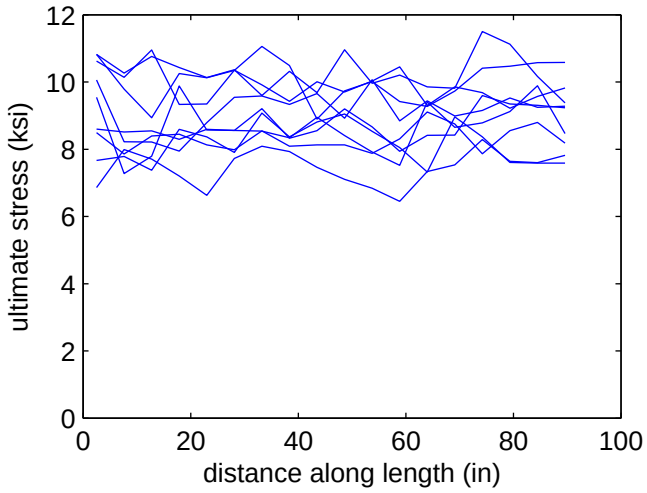

Figure 4.6. Observations of the ultimate stress acting as a random process along the length of Group B.

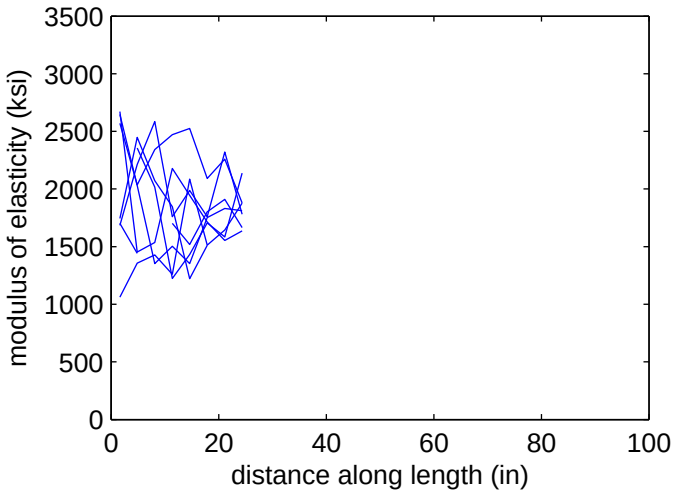

Figure 4.7. Observations of the modulus of elasticity acting as a random process along the length of Group A.

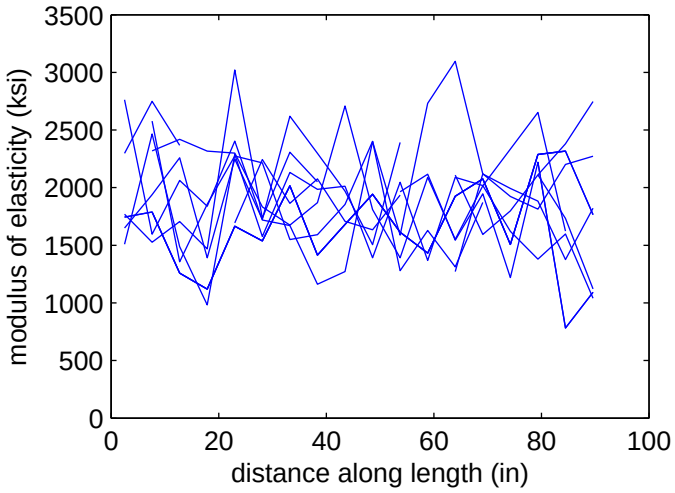

Figure 4.8. Observations of the modulus of elasticity acting as a random process along the length of Group B.

The ensemble estimate of the scaled covariance for the ultimate stress is shown for specimen group A and B in Figures 4.11 and 4.12, respectively, which also includes a summary of the average of the single sample estimations. The ensemble estimate of the auto-covariance for the ultimate stress process for southern yellow pine PSL is shown to be much greater than 20 in for both groups A and B. Single specimen estimations of group B shows some scatter of the correlation length with a very rapid decay. For the single samples the scaled auto-covariance suggests no correlation of strength for any samples at a separation distance of 5 in.

Figures 4.13 and 4.14 below show the sample estimates of the scaled auto-covariance correlation length for the compression modulus of elasticity for specimen groups A and B.

The ensemble estimate of the scaled auto-covariance of the compression modulus of elasticity is shown for specimen groups A and B in Figures 4.15 and 4.16 which also includes a summary of the average of the single sample estimations. The ensemble estimate of the auto-covariance for the elastic modulus for southern yellow pine PSL is shown to be 4 in. which is almost equivalent to the sample spacing. Single specimen estimations of group A and B shows some scatter of the correlation length with a very rapid decay similar to the ensemble auto-covariance. For the single samples the scaled auto-covariance suggests no correlation of modulus of elasticity for any samples at a separation distance greater than 4 in.

For specimen group B the auto-covariance estimates seem to have significantly less scatter than group A which is evident by looking at the single sample estimates for the different groups. Even with deviations of their auto-covariance functions both groups yield similar sample and ensemble estimates of the auto-covariance function. For the compression modulus of elasticity the sample and ensemble estimates converge to an

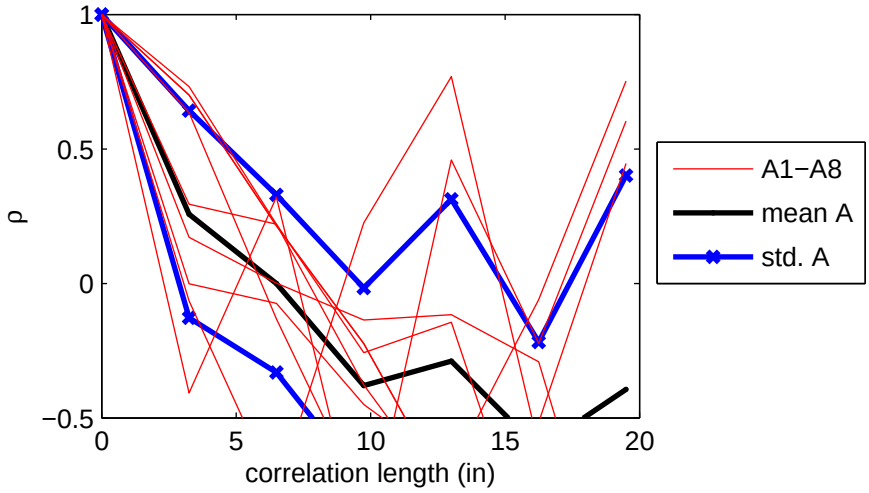

Figure 4.9. Truncated auto-covariance sample estimates of the ultimate stress of southern yellow pine Parallel Strand Lumber for group A.

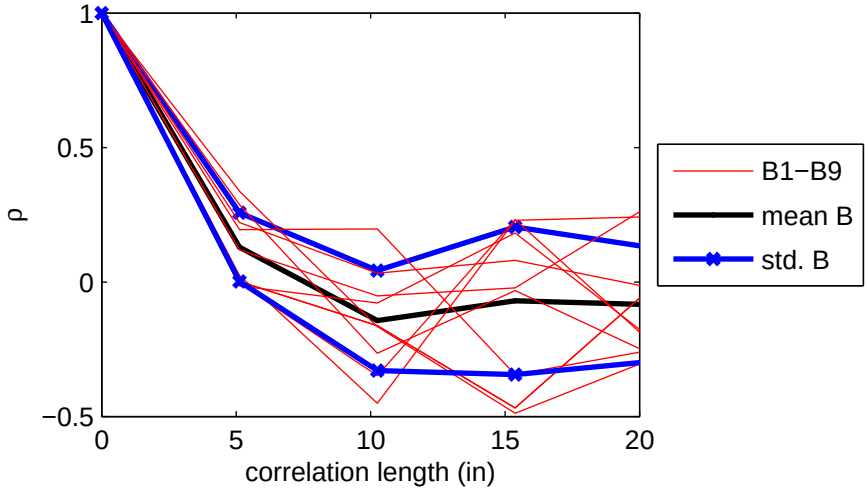

Figure 4.10. Truncated auto-covariance sample estimates of the ultimate stress of southern yellow pine Parallel Strand Lumber for group B.

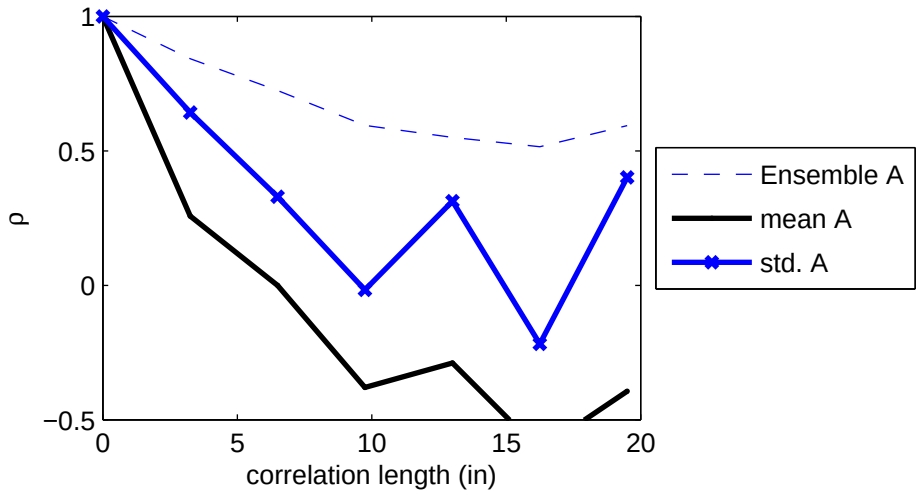

Figure 4.11. Truncated auto-covariance sample estimate average and ensemble average of the ultimate stress of southern yellow pine Parallel Strand Lumber for group A.

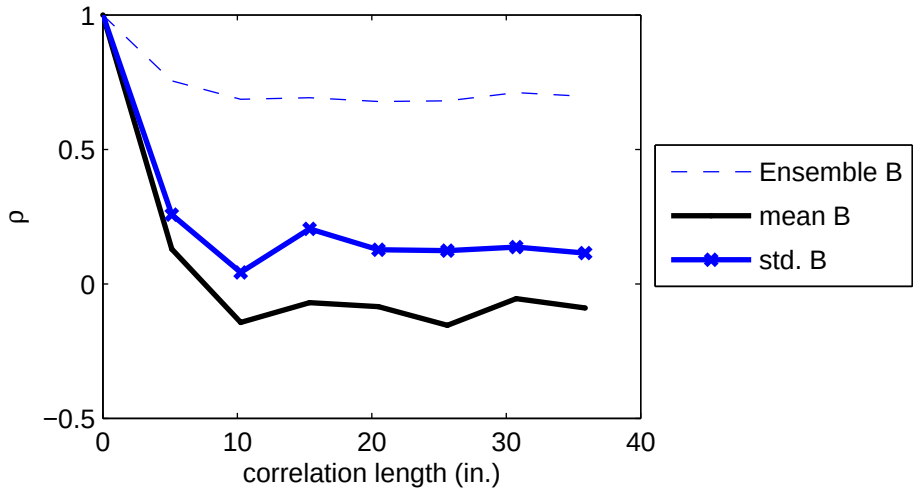

Figure 4.12. Truncated auto-covariance sample estimate average and ensemble average of the ultimate stress of southern yellow pine Parallel Strand Lumber for group B.

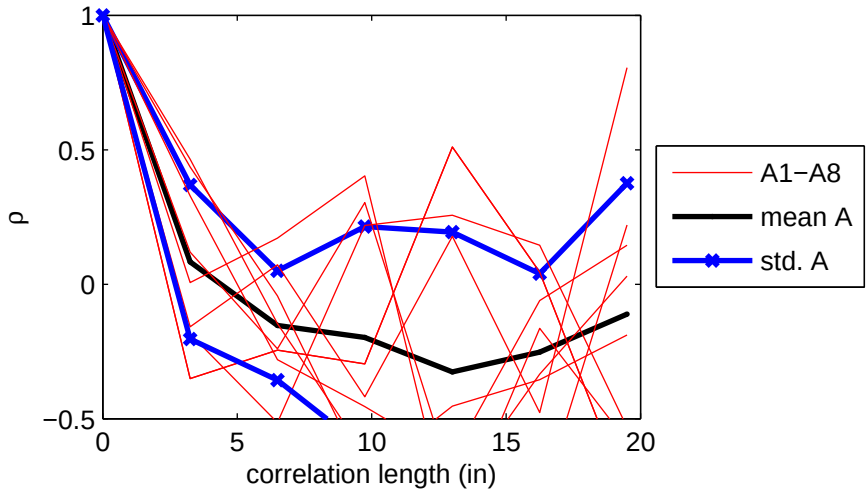

Figure 4.13. Truncated auto-covariance sample estimate average and ensemble average of the compression modulus of elasticity of southern yellow pine Parallel Strand Lumber for group A.

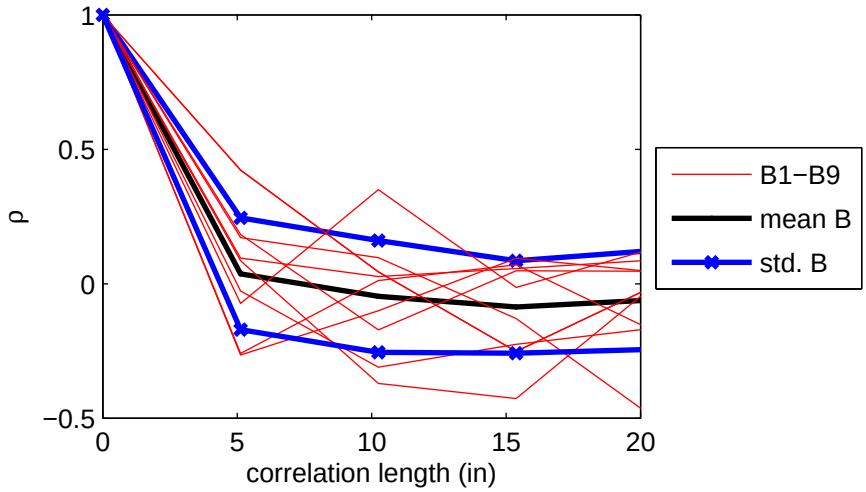

Figure 4.14. Truncated auto-covariance sample estimate average and ensemble average of the compression modulus of elasticity of southern yellow pine Parallel Strand Lumber for group B.

estimate of approximately 4 in. This value does not seem to be a true signature of Parallel Strand Lumber due to the large amount of noise in the compression moduli.

Cross-correlation of the modulus of elasticity for group A specimens is 0.24 and 0.12 for specimen group B. This suggests there is no correlation between the modulus of elasticity and ultimate stress. This value may be under representative of an actual cross-section due to the methods used to obtain estimates of the modulus of elasticity. In the literature review there are no mention of any correlation between these two effective properties in wood.

In small compression samples of Parallel Strand Lumber it is very hard to gather valid estimates of the modulus of elasticity. The method of using an extensometer to measure the strain is very susceptible to any small amount of damage that may occur under loading. These small fluctuations of the extensometer influenced by damage are very hard or unnoticeable when looking graphically at the stress-strain curve, but will have a very large effect when calculating the modulus of elasticity. This variability, which is introduced due to experimental error, causes the sample and ensemble estimates to be very low and invalid. Also, both the small sample pool and experimental error causes the single sample estimates of the correlation length to be very low in both the modulus of elasticity and ultimate stress. Compression tests of this scale seem to give very good estimations of the ultimate stress and its variation, but does not yield very good estimations of the modulus of elasticity and its variation.

4.3 Bending Tests

4.3.1 Overview of Bending Tests

Experimental tests are used to investigate the spatial variation of the bending modulus of Parallel Strand Lumber. Experimental tests are performed on a single member of PSL which is 5.25 in x 5.25 in x 16 ft in dimensions and made from southern yellow pine and on nine 1.55 in x 1.55 in x 8 ft members which are machined from the

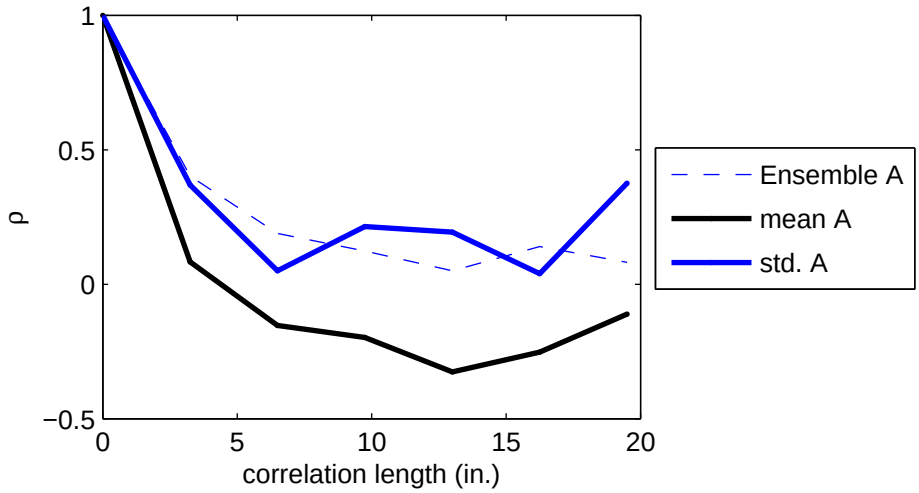

Figure 4.15. Truncated auto-covariance sample estimate average and ensemble average of the compression modulus of elasticity of southern yellow pine Parallel Strand Lumber for group A.

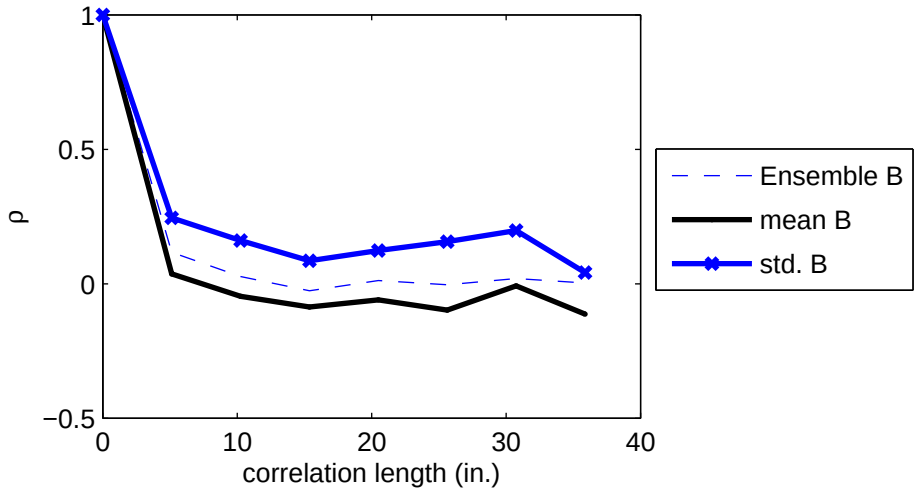

Figure 4.16. Truncated auto-covariance sample estimate average and ensemble average of the compression modulus of elasticity of southern yellow pine Parallel Strand Lumber for group B.

original 5.25 in x 5.25 in x 16 ft member. These experimental tests consisted of a series of three point bending tests which observed the modulus of elasticity as a random process along the length at a series of given points. From this, the mean, variance, and lengthwise auto-correlation of the bending modulus of elasticity is estimated.

The measurements obtained represents a smoothed version of the true modulus field due to averaging of material properties between the three point bending support locations. The goals of these experiments are to estimate a smoothed mean, variance, and auto-correlation of the bending modulus of elasticity.

4.3.2 Method and Results of Bending Tests

To measure the elastic modulus of the Parallel Strand Lumber specimens edgewise bending tests are performed with geometric limits defined by ASTM standard D198-05 to ensure bending dominated behavior. Two specimen groups are used to capture size effects of the averaging of strands in a given cross-section. Specimen A1 is the original section of lumber used in this study and is made from southern yellow pine with a length of 16 ft. After a series of tests described below are performed, nine specimens (B1,B2,...,B9) are machined from specimen A1. Experimental tests are performed with a schematic shown in Figure 4.17, which intends to observe the modulus of elasticity as a random process along the length. Each bending specimen had a total length denoted by L_T, the span between pin-roller support location is L_{sup}, and the spacing of tests along the length of the specimen is L_s. The load P applied at a time step d_t is a user defined constant. Table 4.3 gives the numerical values of each of these parameters below for specimen groups A and B.

Table 4.3. Bending test geometry and parameters.

Group	w (in)	L_T (in)	L_s (in)	L_{sup} (in)	P_{max} (lbs)
A	5.25	192	6	96	500
B	1.55	96	3	15	300

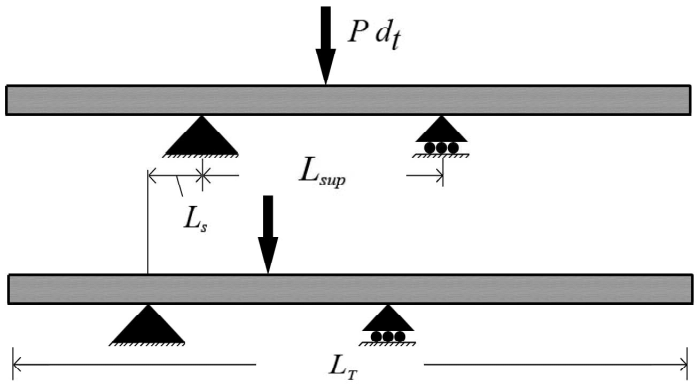

Figure 4.17. Bending test setup schematic showing the passage of a test specimen through two support locations.

These experimental tests were conducted in the Holdsworth Hall wood technology lab at the University of Massachusetts, Amherst using a MTS 30,000 lbs testing device operating in displacement control. These tests were conducted under displacement control at an applied load rate of 0.1 in/min. This rate was used to complete each test between 30 seconds and 3 minutes. Maximum loads were prescribed according to 10% of a given cross-section's size and bending span estimated maximum capacity to ensure there would be no damage to the specimen. During testing the displacement at the mid-span of the test member was measured by a linear variable displacement transducer (LVDT) which was situated under the midpoint of the load application.

These tests were intended to measure the bending modulus of specimens groups A and B and yield a series of mid-span displacements $d(t)$ and applied loads $P(t)$. At each time increment the load can be expressed as

$$P_i(d, E(x), w), x \in \left(x_i - \frac{L_T}{2}, x_i + \frac{L_T}{2}\right] \tag{4.4}$$

where x_i, i = 1,2,...,n are positions along the length of the specimen where the load is applied, $E(x)$ is the averaged effective modulus of elasticity of the cross-section at

position x_i under the load P_i between the two supports which are located respective to position x_i at $a = x_i - \frac{L_{sup}}{2}$ and $b = x_i + \frac{L_T}{2}$.

These experiments related the deflection d_i, load P_i, and moment of inertia $I_{[a,b]}$ to calculate the effective modulus of elasticity between support locations a and b. These parameters are related by

$$d_i = \left[\int \int \frac{m(x_i, u)}{E(x) I_{[a,b]}} \right]_{u=L_T/2} \tag{4.5}$$

where u is an arbitrary variable used for integration which is equal to 0 at one support and L_{sup} at the other, $m(p_i, u)$ is the bending moment induced by the load p, and where $I_{[a,b]}$ is the average moment of inertia between supports a and b which is equal to $I = w^4/12$. The elastic modulus of elasticity is not known and cannot be solved uniquely, instead, it can be replaced by $\hat{E}_{eff,i}$, the effective modulus of elasticity which is defined as $\hat{E}_{eff,i}$=$E(x)$, $x \in \left(x_i - \frac{L_T}{2}, x_i + \frac{L_T}{2}\right]$. Using the deflection formula for a beam under three point bending a solution can be obtained for the effective modulus of elasticity, which is

$$\hat{E}_{eff,i} = \frac{P_{i,t} L_T^3}{48 d_{i,t} I_{[a,b]}} \tag{4.6}$$

where p and d are observed at the same location i, and at the same time t. The hat on the effective or averaged modulus of elasticity between supports a and b denotes experimental noise.

The testing procedure described above yields measurements of the cross-sectional modulus of elasticity at 16 points along the length of specimen group A and 27 points along the length of specimen group B. The raw load verses displacement curves can be seen in Figures 4.18 and 4.19. It should be noted that it appears the group B seems to be stiffer than group A, but that is not a representation of greater material

stiffness, but rather of structural stiffness because of the shorter test span length L_{sup}. By substituting the displacement d with $48dI/L_{sup}^3$ the data is normalized and allows the elastic modulus to be read directly from the slope of the curve. Also, the nonlinear behavior at the lower loads is reflective of seating of the MTS test fixture and not of actual response. To correct this the modulus of elasticity was measured from the linear portion of each test curve manually between loads of 100 lbs and 250 lbs for group B and 100 and 400 lbs for group A.

The results of the testing is shown below in Table 4.4. It is shown from the data that the mean of group A is slightly higher than group B. This higher modulus of elasticity can be attributed to a size effect, where the much smaller 1.55 in x 1.55 in B samples have a greater influence from voids in the cross-section in comparison to the A samples. Also, the standard deviation of sample A1 is significantly lower than group B where the coefficient of variation for A1 is 1.4% and for group B is 9.1%. The amount of variation in a given cross-section is directly proportional to the amount of constitutive strands. For the smaller cross-section there are significantly fewer strands which leads to less averaging of material properties along the length. The test spacing is much less in group B which also leads to less averaging of material properties and a greater variability.

By comparing specimens in group B this data can show the combination of specimen to specimen and within specimen variation. The total standard deviation of all B specimens is 150 ksi and 25 ksi for specimen group A. The standard deviation of the mean value of the effective modulus is 127 ksi for each of the 9 test specimens in group B. This is a measurement of the specimen to specimen variability. The mean value of the standard deviations taken within each sample of the 27 measurements in group B is 98 ksi, which is the magnitude of within-specimen variability of the effective modulus. Based on the data 63% of the total variance can be attributed to specimen to specimen variation and 37% to within specimen variation. The amount of variation

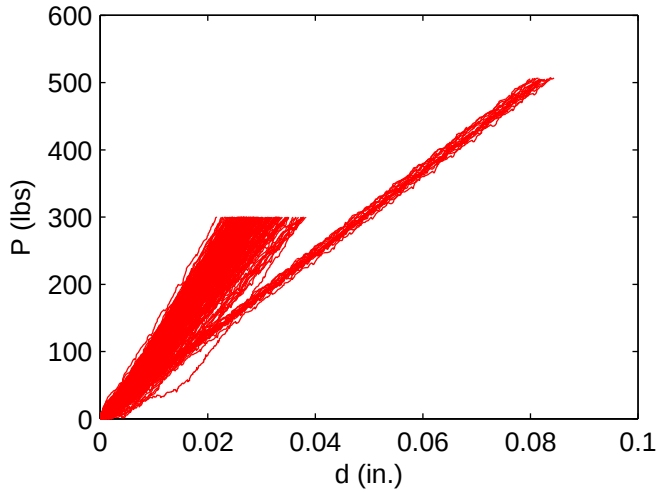

Figure 4.18. Raw load versus displacement curves

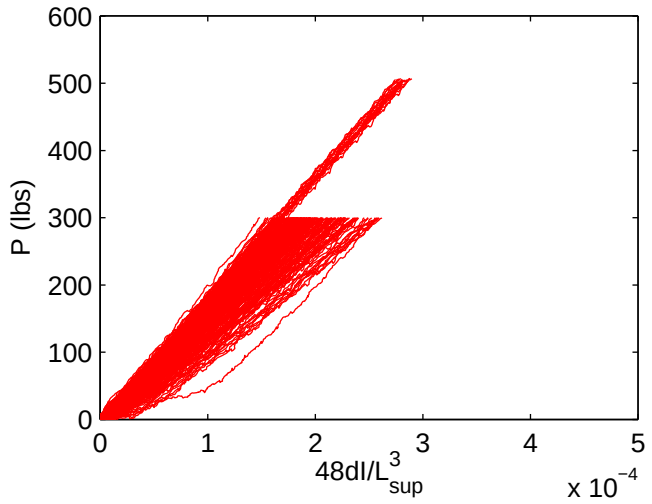

Figure 4.19. Normalized load versus displacement curves

Table 4.4. Bending test results.

Group	mean (ksi)	std. dev. (ksi)
A1	1775	25
B1	1762	110
B2	1826	130
B3	1628	100
B4	1738	82
B5	1673	95
B6	1547	76
B7	1713	84
B8	1493	110
B9	1454	90
B ensemble	1648	150
B means	–	127
B std. devs.	98	–

is shown graphically below in Figure 4.20. From this figure it can be graphically seen that there is both within member and specimen to specimen variation in all of group B specimens. There is only one specimen in group A, but it is shown that there is still within specimen variation and the variability in comparison to group B is much less. It should be observed that these processes appear to be stationary about their respective mean value, while in dimension lumber their modulus of elasticity behaves as a non-stationary process [10][11].

To characterize the spatial variation of the bending modulus of elasticity a formulation for the scaled auto-covariance function was used which is defined as

$$\rho(i,j) = \frac{(\hat{E}_{eff,i} - E[\hat{E}_{eff,i}])(\hat{E}_{eff,i+j} - E[\hat{E}_{eff,i+j}])}{\sigma^2_{\hat{E}_{eff}}} \tag{4.7}$$

where $E[\bullet]$ is the expectation operator, and σ is the standard deviation of the effective modulus of elasticity $\hat{E}_{eff}$ in a single sample or an ensemble of samples. This formulation for the auto-covariance for $\hat{E}_{eff}$ assumes there are n sample observation locations located along the length of a member for which $i = 1, ..., n$. Assuming that

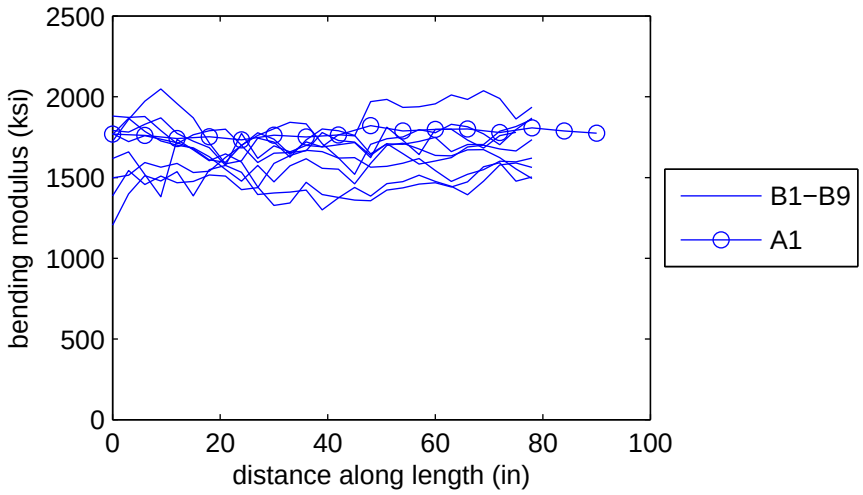

Figure 4.20. Observation of the bending modulus of elasticity as a random process along the length.

the sample spacings are evenly distributed along the length there will be j available locations to estimate the correlation with j defined as the number of samples away from i where j varies from $i, i+1, ..., i+n-1$ with $i+j<n$.

The scaled auto-covariance function of a weakly stationary process can be estimated using both the ensemble mean and single sample mean. If the samples are long enough these two estimates of the auto-covariance will converse to the same values. If the samples are not of significant length or the process is not ergodic, the sample estimations will be substantially different from the ensemble estimate and exact scaled auto-covariance. Within the formulation for the auto-covariance it can be observed that the decay of an ensemble estimate will be substantially less than a single specimen estimate. This is due to the larger number of observations in an ensemble estimate because the length of the samples in these experiments are relatively close to their correlation lengths.

Figure 4.21 below shows the sample estimates of the scaled auto-covariance correlation length for specimen groups A and B. The correlation length L_c of a specimen is defined as

$$L_c = argmax\rho(i,j) : |\rho(i,j)| > exp(-1). \tag{4.8}$$

The ensemble estimate of the scaled covariance is shown for specimen group B in

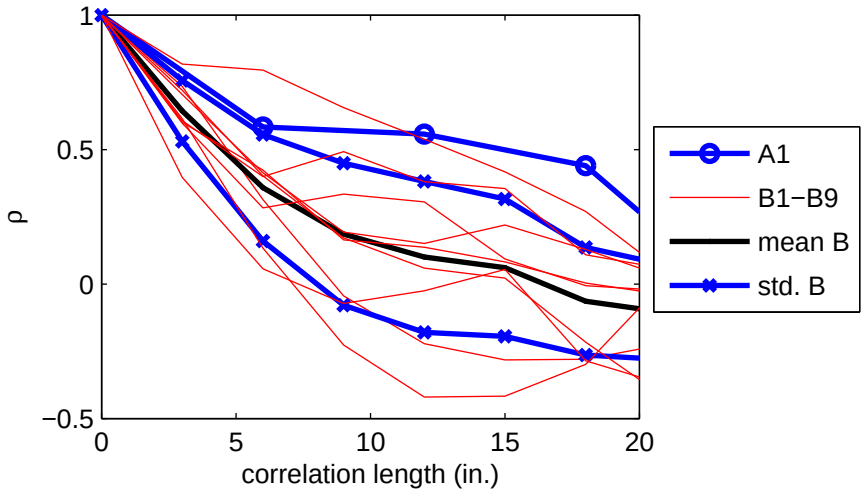

Figure 4.21. Truncated auto-covariance of southern yellow pine Parallel Strand Lumber.

Figure 4.22 which also includes a summary of the average of the single sample estimations. The ensemble estimate of the correlation length for the noisy elastic modulus for southern yellow pine PSL is shown to be approximately 30 in. The abscissa is truncated at a relatively short length due to a larger correlation distance. The sample size is relatively small and the estimation error is dominant. Single specimen estimations of group B show a very large scatter of the correlation length with a very rapid decay. The ensemble estimate of these B samples show a much slower decay. Sample A1 shows less decay than smaller specimens in group B, but no conclusions can be made because of the availability of only one specimen.

These bending experiments provide many estimates of the modulus of elasticity and its variation along the length with very good accuracy. The amount of experimental error seems to average out and is limited by the simplicity of the three point

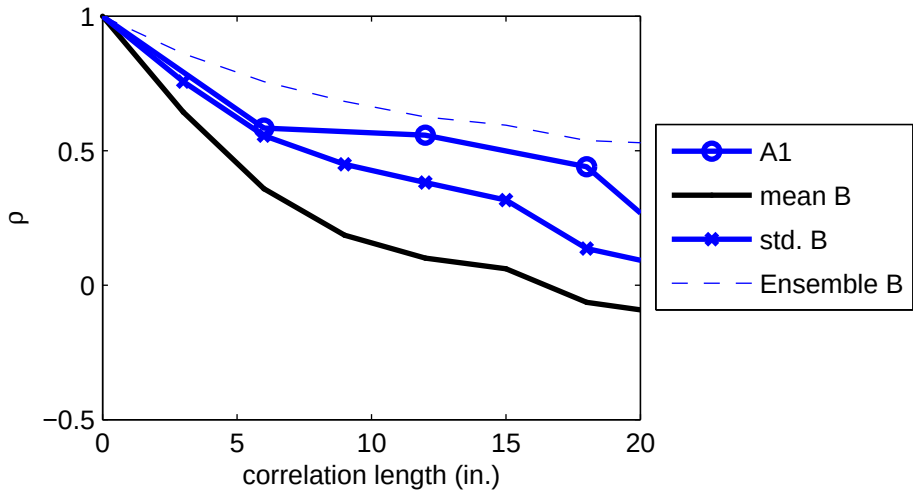

Figure 4.22. Truncated auto-covariance of sample specimen means and ensemble means of southern yellow pine Parallel Strand Lumber.

bending procedure. The bending experiments provided much better estimates of the modulus of elasticity in comparison to the compression tests. This is because the tests experienced little to no seating of the apparatus used and relatively low loads applied. It is very difficult to observe ensemble characteristics of Parallel Strand Lumber due to size limitations on the testing device. In order to achieve this observation much longer samples must be used.

If accurate estimations of the correlation length can be made new procedures in design can be established for testing methodologies for beams or more generally members that experience a tensile stress where the correlation would be most important. By having the correlation length, a weak-link concept can be applied to Parallel Strand Lumber to determine the expected strength of any member with any length.

CHAPTER 5

VALIDATION

5.1 Model Validation Overview

Chapters 2 and 3 describe the models for the mesostructural geometry of Parallel Strand Lumber for the determination of the effective elastic modulus and the ultimate strength of a PSL cross-section. These models are used to simulate Parallel Strand Lumber response which is then compared to the experimental results in Chapter 4. The purpose of these exercises is to validate the computational models.

The parameters described in Chapters 2 and 3 pertain to the geometry of the cross-sections and are set to match that of the experimental tests in Chapter 4. These parameters are listed below in Table 5.1 for the compression specimens and Table 5.2 for bending specimens. The dimensions of each strand cross-section was assumed to have a width of 0.2 in and a depth of 0.5 in. Due to the deterministic strand cross-section size, the simulated cross-sections differ slightly from the actual experimental samples. For the compression specimens it was assumed that there were 12 strands in each cross-section of specimen group A and 24 strands in specimen group B. For the bending specimens it is assumed that there are 270 strands for simulation of specimen group A and 24 strands for simulation for specimen group B. The difference in the overall size due to the deterministic strand size for both specimen groups A and B in bending and compression are less than 0.5%, which is negligible.

The random variables that are used in the computational models are the strand length, elastic constants, plastic constants, and grain angle. These parameters are described in more detail in Chapter 2. The strand length is modeled as a beta random

Table 5.1. Compression test geometry and parameters.

Group	w (in)	d (in)	h (in)	L_T (in)
A	1.10	1.10	3.25	27
B	1.55	1.55	5.00	96

Table 5.2. Bending test geometry and parameters.

Group	w (in)	h (in)	L_T (in)	L_{sup} (in)
A	5.25	5.25	192	6
B	1.55	1.55	96	3

variable. The parameters of the beta distribution for strand length are chosen to be $\alpha = 5$ and $\beta = 2$ and that the interval of strand length is on the fixed interval from 2 ft to 8 ft. This interval was chosen because the strips used in Parallel Strand Lumber are from Plywood scraps which tend to be approximately 8 ft in length. Strands may be broken in the manufacturing process, so a minimum of 2 ft is set. The overall shape of the probability density function can be seen in Figure 5.1. This shows a known bias in the manufacturing process to strands near 8 ft in length. The elastic constants are modeled as Gaussian random variables truncated at zero. Published values of the elastic and strength constants and their coefficient of variations were used in the simulations which are taken from the Wood Handbook (Forest Products Laboratory, 1999). The mean and coefficient of variations for these elastic and strength constants are shown in Table 5.3. It should be noted that these are the full set of elastic and strength constants that are used in the finite element simulations. For the simplified computational models only $E_{x'}$, $E_{y'}$, G_{xy}, ν_{xy}, F_x, F_y, and S_{xy} are needed due to 2D assumptions.

The grain angle is determined from a probability mass function generated from published data [4]. The measurements of grain angles are reported [7] using an automated method for measuring grain angle from x-ray imaging. The models presented here use a previously reported empirical probability mass function for the grain angle

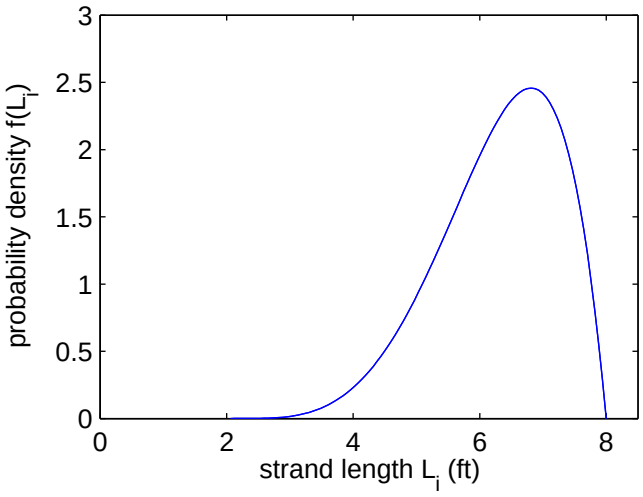

Figure 5.1. Beta random variable probability density function of the strand length.

Table 5.3. Elastic and strength constants and their coefficient of variations.

Constant	mean	coefficient of variation (%)
$E_{x'}$	1886 ksi	20
$E_{y'}$	119.3 ksi	20
$E_{z'}$	203.0 ksi	20
G_{xy}	128.4 ksi	20
G_{xz}	153.9 ksi	20
G_{yz}	13.8 ksi	20
ν_{xy}	0.022	0
ν_{xz}	0.033	0
ν_{yz}	0.634	0
F_x	8.31 ksi	18
F_y	1.75 ksi	18
F_z	1.75 ksi	18
S_{xy}	1.60 ksi	0

for Parallel Strand Lumber [4]. This distribution was obtained from manual measurements of the grain angle by serial sectioning of a Parallel Strand Lumber specimen. For the simulations presented here, the empirical distribution of the measurements is assumed to be characteristic of all Parallel Strand Lumber specimens. It should be noted that this distribution shown in Figure 5.2 is symmetric at zero. It can be observed visually that the majority of the probability mass is concentrated in the interval [0, 10] degrees. This indicates that the majority of the strands are well aligned with the longitudinal axis. Also, there is considerable mass at a grain angle of 90 degrees. This grain angle of 90 degrees is used to represent a strand with a knot defect. These defects significantly weaken the overall strength and also lower the modulus of elasticity of the cross-section.

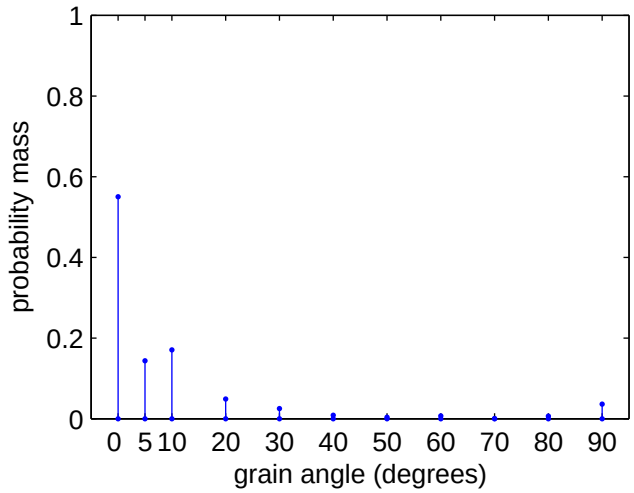

Figure 5.2. Grain angle probability mass function (Clouston, 2006)

5.1.1 Compression Model Validation

Validation of the compression model is attempted by generating 1000 virtual independent samples of specimen groups A and B with equivalent dimensions and total length to that of experimental tests. Virtual specimen samples were extracted from

the full length virtual member at intervals equivalent to the test spacing. From these samples the statistics of the unfiltered modulus and strength processes can be used to yield an estimate of the filtered modulus and strength processes. The unfiltered process is considered to be the true modulus or strength field with no averaging or experimental error introduced. Due to the complexity of formulating a finite element solution that evaluates a series of sections from very long member, just the 2-D simplified method was used to observe the modulus and strength processes along the length. The finite element model was used to verify the mean and coefficient of variation of the modulus of elasticity and ultimate strength. The finite element solutions are also used to observe shear and bond interface interactions, which will be explained in more detail in Chapter 7: Additional Studies. These interactions are neglected using the simplified method which may have a significant influence on the modulus of elasticity and ultimate stress. Only the simplified method results will be validated in this chapter.

The statistics of the 1000 virtual independent samples are shown in Table 5.4 for the ultimate strength and in Table 5.5 for the modulus of elasticity. These tables also include a comparison of the virtual samples and the compression experimental samples. The virtual simulations for the compressive strength slightly under predicts that of the experimental data by 7.2% for specimen group A and 9% for specimen group B. This difference can be attributed to a number of reasons, most notably the strength properties that are being used. Values for the strength parameters used in modeling were from large compression specimens, size effects would cause the compression strength of a cross-section with the dimensions of a strand to be much greater then what was used. The compressive strengths and elastic properties that were used in simulations were that of southern yellow pine. During the manufacturing process a pressure treatment is applied when the material is pressed together to form the Parallel Strand Lumber billet. Also, the simulation assumes that the material

is elastic-perfectly plastic. During the experiments there was some hardening upon yield which could explain a 10-20% increase in the ultimate stress. The standard deviations of the simulated samples were much lower than that of the experimental data by approximately 82% in both specimen groups. The reason for this much lower value is due to experimental error and mix mode failures. During the experimental tests many of the samples experienced mix mode failures. A mix mode failure is defined when crushing and buckling is observed. Several specimens also experienced micro buckling of the outer strands. At loads approximately 60-70% of the ultimate stress, strands would completely or partially delaminate from the specimen and then proceed to buckle soon after. In a few of the other specimens splitting in the interior of the cross-section was noticed and significant buckling of the two halves of the specimen occurred. It should be noted that neglecting within strand variations decreases the variability of these small samples dramatically due to the very short sample lengths which can account for a large difference in the variability.

The sample estimates for the compression modulus of elasticity do not agree well with the experimental data. The virtual tests under predict the modulus of elasticity by 16% and 18% for specimen groups A and B respectively. Also, the modulus of elasticity estimates under predict the standard deviation by 72% and 233%. This significant disagreement between results is most likely due to the method of obtaining the modulus of elasticity from experimental results. The modulus of elasticity was taken from the stress-strain curves for each specimen. This methodology is very subjective to where the slope was taken on the graph, which is a direct cause of the large standard deviation for the experimental results. Also, additional variability in the experimental data is likely due to mix mode laminate failure, where in solid dimensioned wood, most failures will occur by crushing.

The next goal of this validation is to compare the auto-covariance of the modulus of elasticity and ultimate stress of specimen groups A and B to the simulated

Table 5.4. Virtual simulation of the ultimate compressive strength for specimen groups A and B with a comparison to the experimental data.

		virtual A	virtual B	exp. A	exp. B
ensemble	mean (ksi)	7.19	7.18	7.71	8.97
	std. dev. (ksi)	0.20	0.25	1.09	1.02
	skewness	-0.94	-0.04	0.10	0.05
	kurtosis	14.3	2.98	2.35	2.54
sample	mean of std. devs. (ksi)	0.65	0.46	1.01	0.96
	std. dev. of means (ksi)	0.04	0.01	0.55	0.53

Table 5.5. Virtual simulation of the modulus of elasticity for specimen groups A and B with a comparison to the experimental data.

		virtual A	virtual B	exp. A	exp. B
ensemble	mean (ksi)	1580	1573	1840	1860
	std. dev. (ksi)	174	120	300	400
sample	mean of std. devs. (ksi)	55.5	66.3	–	–
	std. dev. of means (ksi)	5.60	1.57	220	151

data. Figures 5.3, 5.4, 5.5, and 5.6, show a graphical comparison of the ensemble mean, sample mean, and standard deviation of the auto-covariance estimates at different separation distances. Graphically it can be shown that the ensemble and sample means of the experimental filtered modulus process and unfiltered simulated modulus differ significantly. The compression ultimate stress agrees well with the experimental data. The procedure in which the compression modulus of elasticity is obtained introduces significant errors into the process along the length and it cannot be easily compared to simulated data. These errors are introduced by seating of the cross-head into the specimens and also small damage drastically effecting the strain measurements by the extensometer. The ultimate stress for both specimen groups A and B agree very well with simulated results. The short test spacing causes the filtered and unfiltered processes to converge because there is little to no averaging over such short distances in the process. In addition the small number of strands yields little to no averaging as well. The estimations of the cross-correlation of the

modulus of elasticity and ultimate stress are 0.58 for the A specimens and 0.62 for the B specimens. This suggests there is some correlation which is not observed in the experimental results. This cannot be readily explained, but may be from a strain based approach using the modulus of elasticity values to calculate the strain at failure of each strand.

Figures 5.3, 5.4, 5.5, and 5.6 show examples of the unfiltered and filtered modulus of elasticity and ultimate stress processes. The samples of the unfiltered modulus and ultimate stress are piecewise constant due to the assumption that there is no within strand variation. This means, segments where there are no strands ending have constant elastic properties, which is more easily shown in Figures 5.7 and 5.8 for the compression simulated data because these simulations have the least number of strands in a cross-section.

For the simulated compression samples, the unfiltered and filtered processes are very similar. For small cross-sections and short lengths, the amount of variation within a cross-section is minimal due to the simplification that each strand has constant properties along its entire length. Although there are very few strands within a cross-section, the effect that ending and beginning strands with different properties have, causes very large fluctuations in the standard deviation and the compression modulus or peak stress. This is evident in the very large coefficient of variation of the modulus of elasticity and ultimate stress in both simulated and experimental data. The filtering of the effective properties has little affect on the modulus or ultimate stress process along the length due to the specimen spacing being much less than the assumed average strand length. It can also be assumed that the majority of the specimens at a length of 5.0 in or 3.25 in have no strands ending within that spacing. This is because the majority of the strands are on the interval from 2 to 8 ft in length with the majority of them being closer to 8 ft in length. The maximum length tested was 8 ft in length. This is observed in the experimental specimens as well.

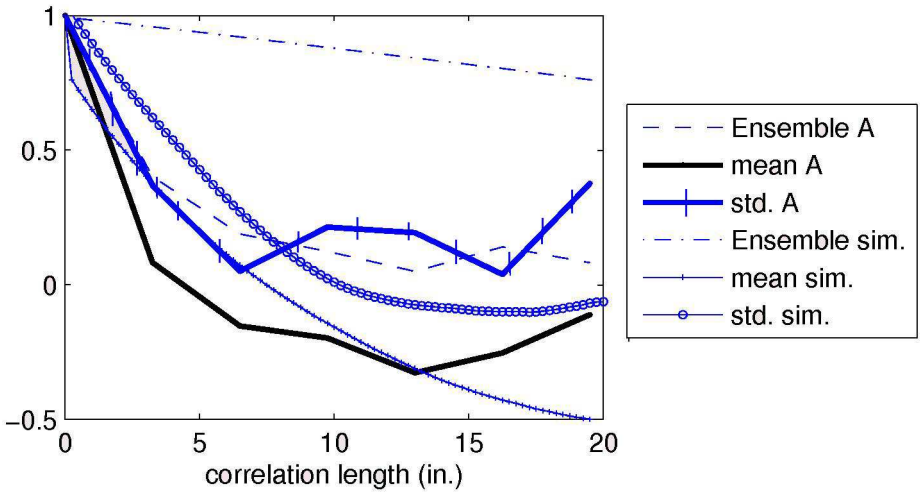

Figure 5.3. Observations of the compressive modulus of elasticity auto-covariance as a function of separation distance of Group A for simulated and experimental data.

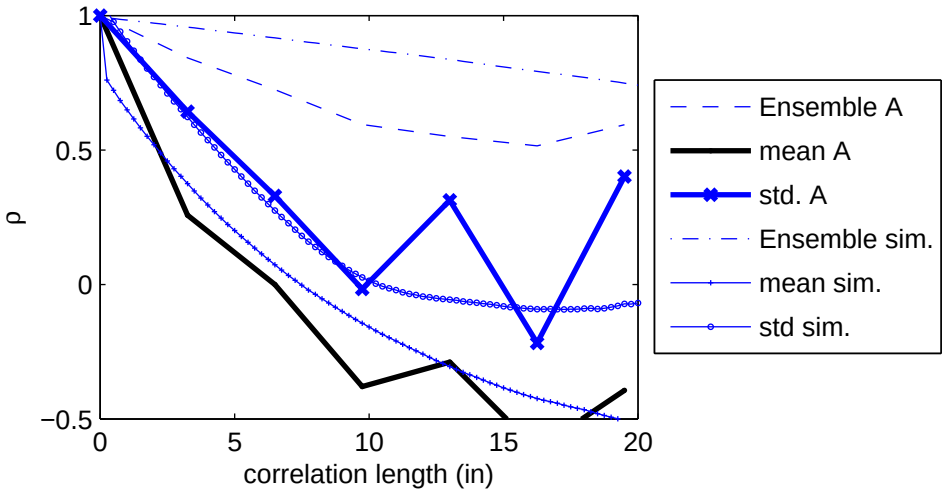

Figure 5.4. Observations of the ultimate stress auto-covariance as a function of separation distance of Group A for simulated and experimental data.

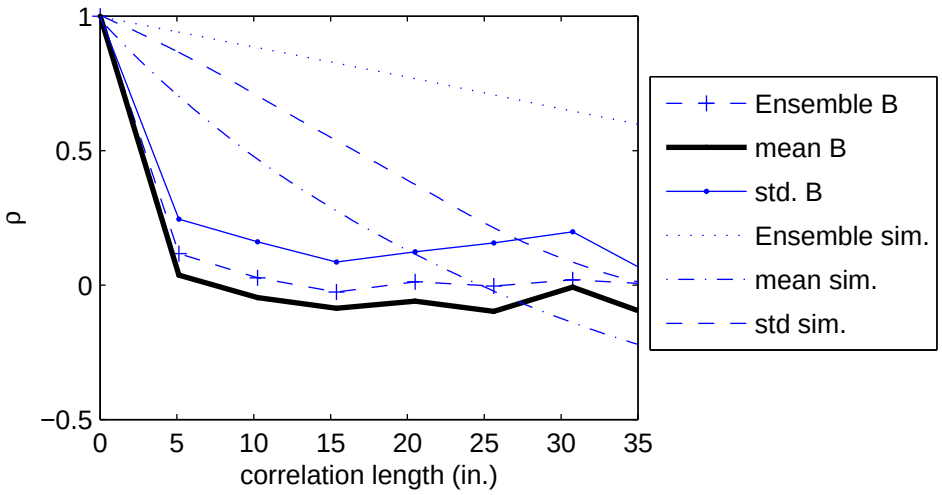

Figure 5.5. Observations of the compressive modulus acting as a random process along the length of Group B for the simulated and experimental data.

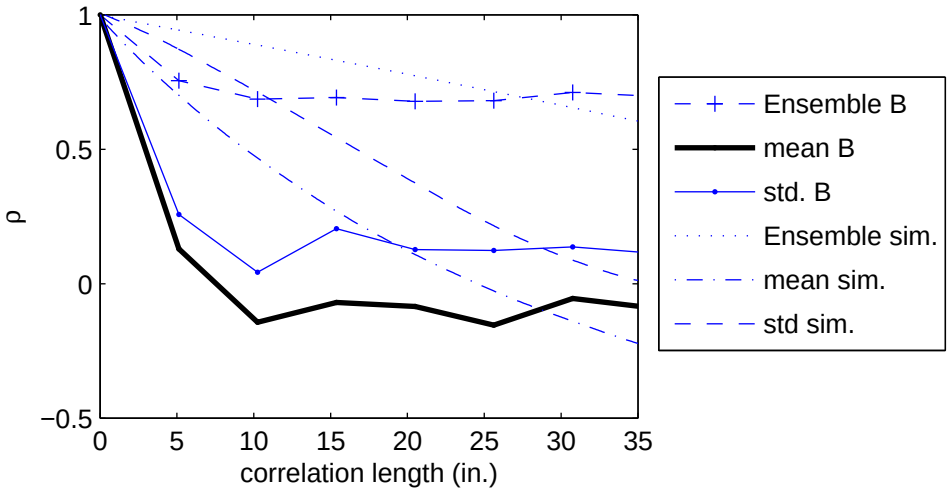

Figure 5.6. Observations of the ultimate stress acting as a random process along the length of Group B for the simulated and experimental data.

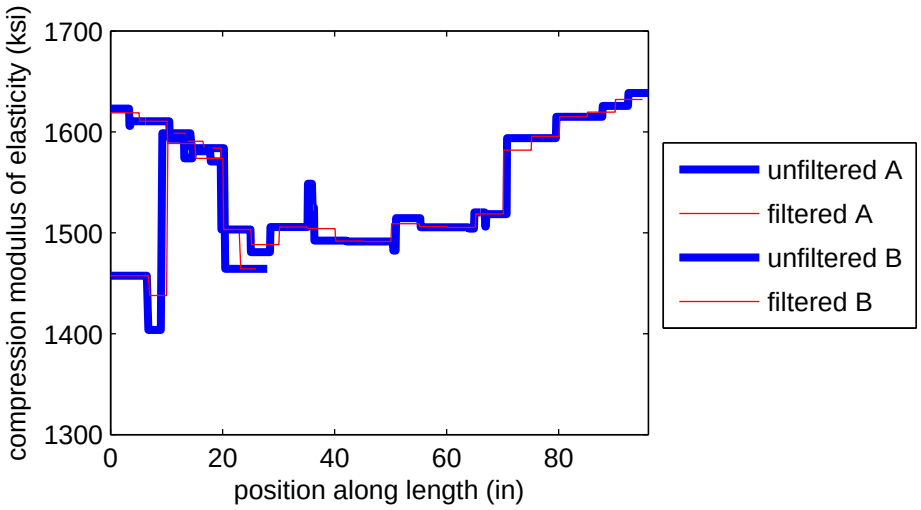

Figure 5.7. Observations of the compressive modulus of elasticity acting as a moving process along the length of Groups A and B for the simulated unfiltered and filtered processes.

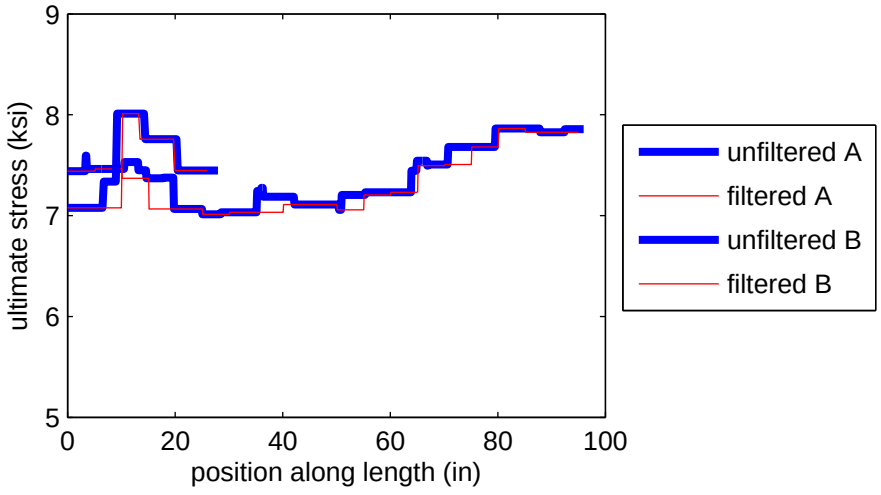

Figure 5.8. Observations of the ultimate stress acting as a moving process along the length of Groups A and B for the simulated unfiltered and filtered processes.

5.1.2 Bending Model Validation

Validation of the bending model is attempted by generating 250 virtual independent samples of specimen groups A and B. From these samples the statistics of the unfiltered modulus process can be used to yield estimates of the filtered modulus process. Finite element solutions were also performed which were used to verify and give estimates of the mean and coefficient of variation of the modulus of elasticity and ultimate stress. These results are explained in more detail in Chapter 7: Additional Studies. Only the 2-D simplified method will be reported in this section.

The statistics of the 250 virtual independent samples are shown in Tables 5.6, which includes a comparison of the virtual samples and the experimental samples. The most direct comparison can be made between the samples of specimen group B. In total there were 9 experimental B samples tested. The virtual tests under predict the modulus of elasticity by 11% and under predicts the standard deviation by 38%. For a material such as wood this amount of variation is normal, and the agreement between the predicted and measured ensemble means are good. The variability of the virtual samples being under predicted is excepted due to the omission of voids, within strand variation, and also the size of voids considered in the model. Also, experimental error will increase the variability, as well as, the method for extracting the modulus of elasticity from the load-displacement relationships given by the load cell and LVDT.

The sample estimates for group B agree with the experimental data in that the mean of the standard deviations for the sample estimates are less than the ensemble estimate of the standard deviation. For the virtual samples the sample standard deviation is 81% of the ensemble standard deviation. For the experimental data the sample standard deviation is 65% of the ensemble standard deviation. These simulations yield similar results with the experimental data suggesting that the individual

sample lengths are insufficiently long to capture the actual spatial variability of Parallel Strand Lumber.

For specimen group A the experimental pool size is too low to give a reasonable comparison to simulated results. The mean value for specimen group B is equivalent to that of the virtual A samples. The standard deviation agrees well with the experimental value having a value 5% less than the virtual samples. The ensemble statistics cannot be readily compared due to only one experimental data set available for specimen group A.

For both the experimental and virtual samples the kurtosis and skewness show that a Gaussian representation of the data is applicable.

Table 5.6. Virtual simulation of bending tests for specimen groups A and B with a comparison to the experimental data.

		virtual A	virtual B	exp. A	exp. B
ensemble	mean (ksi)	1569	1572	1775	1648
	std. dev. (ksi)	26.3	94	25	150
	skewness	0.017	0.16	–	0.038
	kurtosis	2.50	3.17	–	2.80
sample	mean of std. devs. (ksi)	36	116	–	127
	std. dev. of means (ksi)	22.8	65	–	98

The next goal of this validation is to compare the modulus of elasticity of specimen group B to the simulated data. Computational models are not validated using specimen A1 due to only one data set available. The bending modulus of elasticity process is shown in Figure 5.9. The effect of filtering is more apparent due to more averaging in the bending specimens then the compression specimens. Even with the filtering effect, the relatively short test spacing causes the data to be in good agreement with for ensemble and sample estimates.

Figure 5.10 show examples of the unfiltered and filtered process of the modulus of elasticity for specimen groups A and B in bending. The filtering effect is most

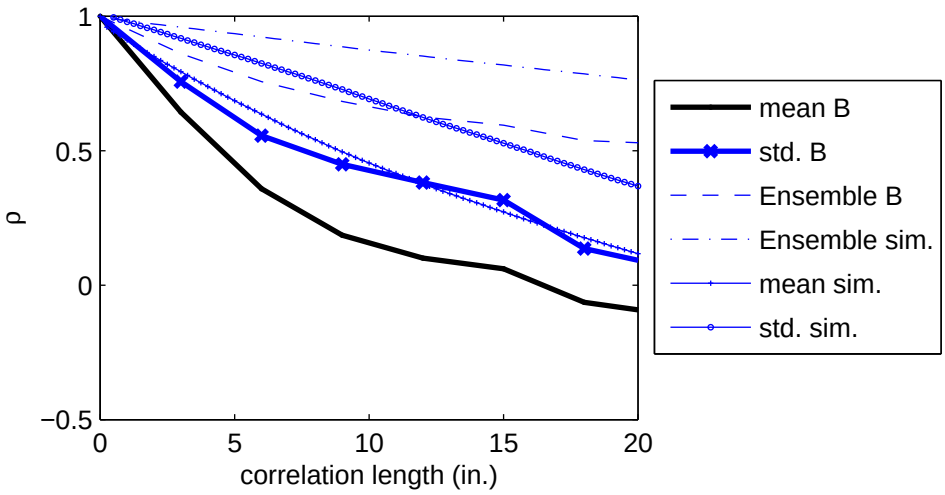

Figure 5.9. Observations of the bending modulus of elasticity auto-covariance as a function of separation distance of Group B for the simulated and experimental data. Simulated data with noise is not included in this figure.

evident in specimen groups A and B of the bending samples in Figure 5.10. The A samples have an 8 ft span, which averages the properties over a much greater volume of material then the smaller B samples which has a bending span of only 15 in. The samples of the unfiltered modulus and ultimate stress are piecewise constant due to the assumption that there is no within strand variation. This means, segments where there are no strands ending have constant elastic properties, which is more easily shown in Figures 5.7 and 5.8 for the compression simulated data. This is because these simulations have the least number of strands in a cross-section and the shortest model lengths.

Specimen group A of the bending modulus of elasticity process shows very small piecewise segments due to the large number of strands in a given cross-section. Because of this there are a significant number of strands ending along the member which cause rapid changes in the peaks in comparison to specimen group B of the bending modulus of elasticity. Even though there are significant numbers of strands ending

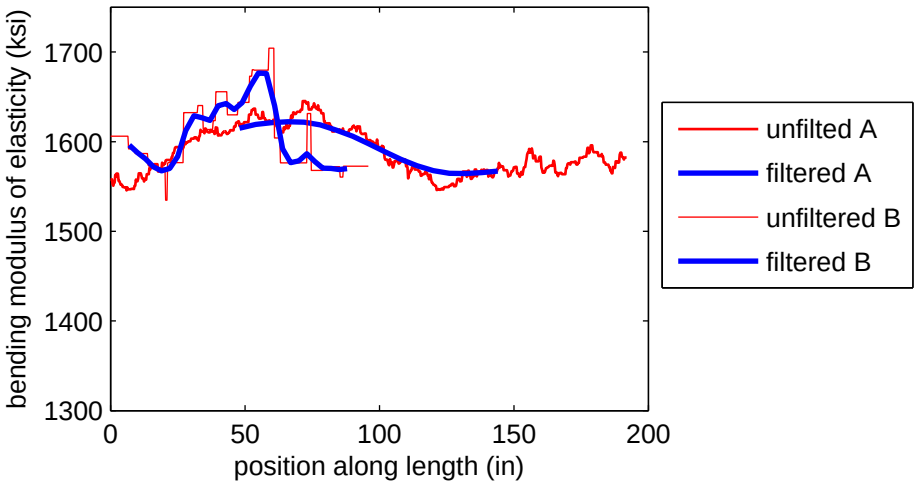

Figure 5.10. Observations of the bending modulus of elasticity acting as a moving process along the length of Groups A and B for the simulated unfiltered and filtered processes. Simulated data with noise is not included in this figure.

along the member these properties average out because of the large number of total strands in a cross-section.

These figures give insight into how averaging can affect the modulus of elasticity process. For the bending specimens of group B small test spacing results in the averaging effect becoming negligible. This is evident with the unfiltered and filtered processes being very similar. For specimen group A the very large span results in significant averaging which causes the unfiltered and filtered processes to have dramatically different properties in both the standard deviation and also the shape of the random process. Most peaks and noise in the data are smoothed out which can lead to false interpretation of the actual properties along the length of a given section. These results indicate that one should be very careful when determining the spatial statistics of bending specimens as averaging may lead to inaccuracies. If one is to determine these statistics they should use as short of a span as possible to limit the averaging which will more closely represent the true spatial characteristics of the bending modulus of elasticity. This span should also limit appreciable shear deformations.

5.1.3 Conclusion of Validation

The simulated data can be validated by the experimental results for the bending modulus of elasticity and the ultimate stress. The effective properties and correlation lengths are very similar between the simulated and experimental data with some under prediction of the variation due to the neglect of within strand variability. For the compression modulus of elasticity the validity of the experimental data is questionable and hard to make any concluding remark whether the simulated data is also valid. Using solid wood as a high end value for the coefficient of variation of the modulus of elasticity which is 20% [8], values obtained for the coefficient of variation in the experimental section were between 17-21%. For Parallel Strand Lumber the amount of variation is much less due to the averaging of material properties, so, simulated compression moduli having a coefficient of variation between 8-11% seems valid.

CHAPTER 6

SIMULATION RESULTS

6.1 Simulation Overview

Having validated the computational model in the previous chapter, the simulations of the bending modulus of elasticity, compression modulus of elasticity, and ultimate stress were used to derive a probabilistic characterization of the filtered random processes of the experimental data. A second set of simulations were performed on specimens having the same cross-section dimensions as the ones used in Chapter 5: Validation, defined below in Tables 6.1 and 6.2, but with a much longer length as to allow for capturing of the full decay of the auto covariance. 1000 A' and 1000 B' compression specimens and 250 A' and 250 B' bending specimens are generated and analyzed using 2-D computational models. The new lengths are also shown below in Tables 6.1 and 6.2.

Table 6.1. Compression simulation geometry and parameters. The values in the parenthesis are the dimensions of the experimental tests.

Group	w (in)	d (in)	h (in)	L_T (in)	simulations	num. strands
A	1.00(1.10)	1.00(1.10)	3.25(3.25)	720(27)	1000(8)	12(-)
B	1.50(1.55)	1.60(1.55)	5.00(5.00)	720(96)	1000(9)	24(-)

6.2 Compression Simulation Results

Tables 6.3 and 6.4 show the point statistics of the ultimate stress and compressive modulus of elasticity. The unfiltered and filtered processes for the compression samples A' and B' yield nearly identical results. By observing the skewness and kurtosis

Table 6.2. Bending simulation geometry and parameters.

Group	w (in)	h (in)	L_T (in)	L_{sup} (in)	simulations	num. strands
A	5.00(5.25)	5.40(5.25)	600(192)	6(6)	250(1)	270(-)
B	1.50(1.55)	1.60(1.55)	600(96)	3(3)	250(9)	24(-)

of the data the specimens in both compression and bending appear to have a near Gaussian distribution. By comparing the standard deviations it can be shown that the increasing number of strands decreases the variability.

Both the $E(x)$ modulus and $S(x)$ ultimate stress processes are assumed to be weakly stationary and ergodic. The statistics in Tables 6.3 and 6.4 give insight that the marginal distribution of S(x) and E(x) is Gaussian. This model is appropriate because the formulation of the effective modulus of elasticity and ultimate stress are a summation of independent identically distributed random variables in compression. By assuming the central limit theorem holds a Gaussian probabilistic model can be used to represent the simulated data. It should be noted that this model can only be applied to cross-sections having more than 15 strands as sections with fewer strands than this tend be behave as a non-Gaussian distribution. Evidence of this is shown in the simulation of 1000 cross-sections with 12 strands and a total length of 27 in., where the kurtosis was 13.6 for the modulus process and 14.3 for the strength process. The skewness of these processes are -0.58 and -0.94, respectively, where a Gaussian model would not be appropriate.

Figure 6.1 shows the scaled auto-covariance processes for specimen groups A' of the ultimate stress. The compression modulus of elasticity and B' ultimate stress processes are similar, but not shown, with a linear scaled auto-covariance to 0 and then constant at a value approximately 0 at further increments of length.

It is interesting to compare the different correlation lengths which are defined as

$$L_c = \text{argmax}\rho(i,j) : |\rho(i,j)| > exp(-1). \tag{6.1}$$

The size of the cross-section and the amount of averaging present have a large effect on the overall correlation length. For the compression specimens the unfiltered and filtered processes have nearly identical correlation lengths. Slightly longer correlations are noted for both the A' and B' specimen groups due to some averaging. The ensemble and sample correlation lengths differ by approximately 10% in all cases. The cross-correlation of both A' and B' specimen groups are 0.68 and 0.67, respectively. This suggests there is some correlation between the strength and the modulus of elasticity. This correlation between the strength and modulus of elasticity may be a result from the calculation of the stress in each strand being calculated using the modulus of elasticity of the strand.

Table 6.3. Point statistics of the filtered and unfiltered simulated ultimate stress processes.

Statistic	A' unfiltered	A' filtered	B' unfiltered	B' filtered
mean (ksi)	7.17	7.13	7.17	7.13
std. dev. (ksi)	0.61	0.61	0.43	0.43
skewness	-0.13	-0.12	-0.09	-0.08
kurtosis	2.59	2.58	2.65	2.64
corr. length ensemble (in)	55.8	56.3	55.3	55.8
corr. length sample (in)	50.3	50.7	49.7	50.0

6.3 Bending Simulation Results

Table 6.5 show the point statistics of the bending modulus of elasticity. Some filtering can be seen in the B' samples which is evident by a small reduction in the standard deviation. Significant averaging can be seen for the A' bending specimens. This is due to the 8 ft span for the B' where more averaging occurs in comparison

Table 6.4. Point statistics of the filtered and unfiltered simulated compression modulus of elasticity processes.

Statistic	A' unfiltered	A' filtered	B' unfiltered	B' filtered
mean (ksi)	1572	1572	1571	1571
std. dev. (ksi)	159	157	111	110
skewness	-0.13	-0.13	-0.08	-0.08
kurtosis	2.59	2.58	2.63	2.62
corr. length ensemble (in)	56.0	56.3	56.5	57.0
corr. length sample (in)	50.4	50.9	49.7	50.2

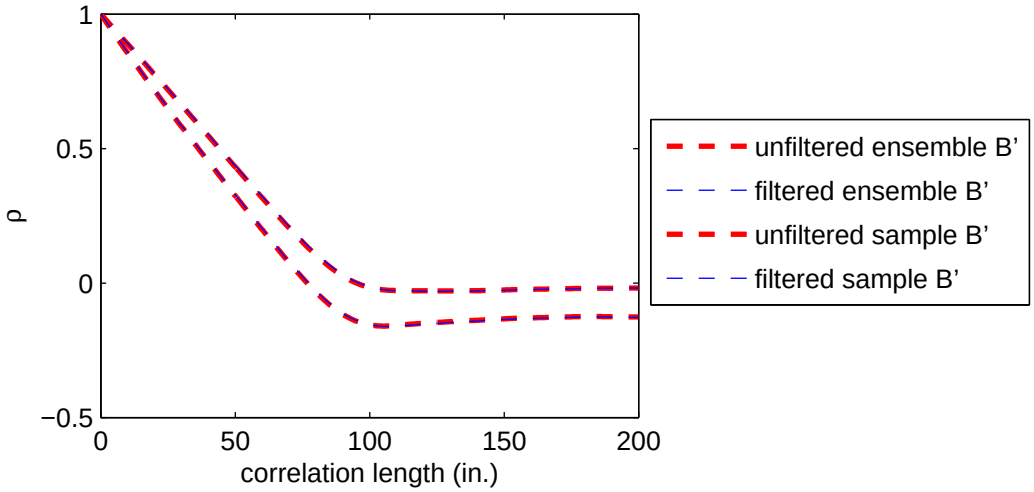

Figure 6.1. Comparison of the unfiltered and filtered auto-covariance functions of 1000 simulated 1.55 in x 1.55 in x 720 in members.

to the smaller A' span of 15 inches. By comparing the standard deviations it can be shown that the increasing number of strands decreases the variability. The standard deviation of the A' samples is 32.1 ksi and the B' samples have a standard deviation of 112 ksi.

The $E(x)$ modulus of elasticity process is assumed to be weakly stationary and ergodic. The statistics in Table 6.5 give insight that the marginal distribution of E(x) is Gaussian. It is interesting to then compare the correlation lengths which are defined as

$$L_c = \text{argmax}\rho(i,j) : |\rho(i,j)| > exp(-1). \tag{6.2}$$

The size of the cross-section and the amount of averaging present have a large effect on the overall correlation length. The filtering effect is noticed more in the bending modulus of elasticity A' and B' specimen groups. The A' samples have a difference in the correlation length of 9.5 in which is significant. This is due to the large bending span which causes many peak values to be averaged out. The B' specimens, which are significantly smaller in cross-section and have a shorter test span, have an unfiltered correlation length 3 in smaller than the filtered correlation length. The ensemble and sample correlation lengths differ by approximately 10% for the A' and B' samples.

Table 6.5. Point statistics of the filtered and unfiltered simulated bending modulus of elasticity processes.

Statistic	A' unfiltered	A' filtered	B' unfiltered	B' filtered
mean (ksi)	1572	1572	1571	1570
std. dev. (ksi)	32.1	27.2	112	110
skewness	-0.02	-0.02	-0.10	-0.09
kurtosis	2.62	2.44	2.60	2.57
corr. length ensemble (in)	56.5	66	57.0	60.0
corr. length sample (in)	48.5	58.0	49.2	51.8

6.4 Simulation Results Summary

Based upon the validation study and the further simulations of this chapter, many important features about testing and simulation can be concluded. For typical experiments, compression samples have a fairly small cross-section and short length. For solid wood testing this is ideal because it makes testing fast and yields very accurate results for both the modulus of elasticity and ultimate stress. For Parallel Strand Lumber there are many drawbacks from having such a small cross-sectional

size. This cross-sectional size causes many unwanted failure modes such as the delamination of the outer strands. A nominally sized member, such as one used for a column in a wood framing structure, the delamination of several strands will have little effect on the shape of the stress-strain curve, the modulus of elasticity, and ultimate stress. When there are only 12-24 strands within a cross-section the unwanted failure of these strands can have a significant effect on the covariance, modulus of elasticity, and ultimate stress. The only alternative to this testing is to have much larger cross-sections, but this will put very high stresses on the testing machine or surpass its capacity. One possible fix is to filter the data based on certain failure modes, which would remove data that underwent a failure mode that would not be characteristic of a typically sized member used in an engineering application. If full scale members are used, the spatial correlation could not be easily obtained because of the filtering effect which is not apparent in smaller compression specimens. From the simulations based in this chapter it is easy to create a variety of easy to implement sample generation techniques which will be presented in Chapter 7: Additional Studies. Models of significant length give good representations of the experimental data. The overall agreement between the experimental tests and the simulated data is very good. Initial models suggest that the length of the specimens are still too short to capture the spatial correlation and much longer samples should be used. The covariance of the experimental and simulated data differ significantly in compression. This is mainly due to the small cross-sections and the neglect of within strand variation. For the longer A' and B' simulations the within strand variation is very insignificant in comparison to the length-wise variability. These specimens give a much better representation of how the number of strands in a cross-section effect the variability of the members.

For the bending experiments, researchers should be wary about the cross-sectional size and test span used. Ideally the cross-section should be as small as possible to allow

as short bending spans as possible without significant shear deformations. For large cross-sections and bending spans the filtering causes the variability of the modulus of elasticity to be much lower then what it actually is. This is most evident in the A' bending specimens where the standard deviation is reduced by 12.5%.

Overall the experimental tests were too short to provide accurate correlation distances at long separation distances. By simulating A' and B' specimens of large length it yields very accurate correlation lengths and statistics about Parallel Strand Lumber. The compression and bending tests have converging ensemble and sample estimates of the correlation length which are approximately 56 in.

CHAPTER 7

ADDITIONAL PARAMETER STUDIES

7.1 Overview

The objective of these additional studies are to expand upon computational results presented in in Chapter 5: Validation and Chapter 6: Results.

7.2 Stiffness and Strength Parameters

7.2.1 Study of the Modulus of Elasticity and Ultimate Stress versus the Number of Strands and Cross-sectional Size

The cross-sectional size and number of strands have a direct effect on both the probability model that can represent the data and variation of the modulus of elasticity and ultimate stress. By generating cross-section cuts with an increasing number of strands and performing an analysis of how the effective properties change, it is possible to get a direct relationship between the number of strands and coefficient of variation of the modulus of elasticity or ultimate stress.

For the modulus of elasticity, the number of strands in the simulations ranged from one to 300. This range was chosen to capture the effect of the modulus of elasticity on a broad range of cross-sections which includes sizes of the experimental cross-sections. In total there are 1000 observations of the modulus of elasticity for each number of strands from 1 to 300, where an illustration of these simulations are shown in Figure 7.1. This figure limits the data set to better show the variability. When the number of strands is between approximately 1 and 15 there is a significant increase in the standard deviation. The distribution of moduli also become non-Gaussian as

the Central Limit Theorem does not apply. As the amount of strands increases the variability decreases which is shown in Figures 7.1 and 7.2 and the moduli behave as a Gaussian distribution.

For a large number of strands, the standard deviation nearly converges to approximately 0 ksi because the effect of one additional strand is negligible on the modulus of elasticity. Figure 7.2 shows a representation of how the modulus of elasticity varies with cross-section size. Figures 7.3, 7.4, 7.5, 7.6, 7.7, and 7.8 show the transformation of the modulus of elasticity observations into a Gaussian data set. As shown in previous chapters the modulus of elasticity of the 1.10 x 1.10 in and 1.55 in x 1.55 in cross-sections used in the experiments has much greater variability in comparison to the larger 5.25 in x 5.25 in cross-section.

The relationship between the standard deviation σ_E and number of strands is

$$\sigma_E = \frac{592.5 \text{ ksi}}{\sqrt{n_s}}. \tag{7.1}$$

The relationship between the standard deviation σ_E and the cross-sectional dimensions for a fixed strand size is

$$\sigma_E = \frac{711.8 \text{ ksi}}{n_s wd \text{ in}^2}. \tag{7.2}$$

A similar set of simulations are performed to determine how the ultimate stress varies with an increasing number of strands and cross-section size. The amount of simulations is reduced to 100 for each number of strands and only brought out to a total number of strands of 30. This interval and number of simulations are chosen because these simulations takes significantly longer time to run than the modulus of elasticity simulations. From Figures 7.9 and 7.10 it can be shown that the ultimate stress has a similar decay in the variability of the ultimate stress with an increasing cross-sectional size. The amount of variation is greatest when there are very few strands in the model. The ultimate stress data has a slower decay of the variance

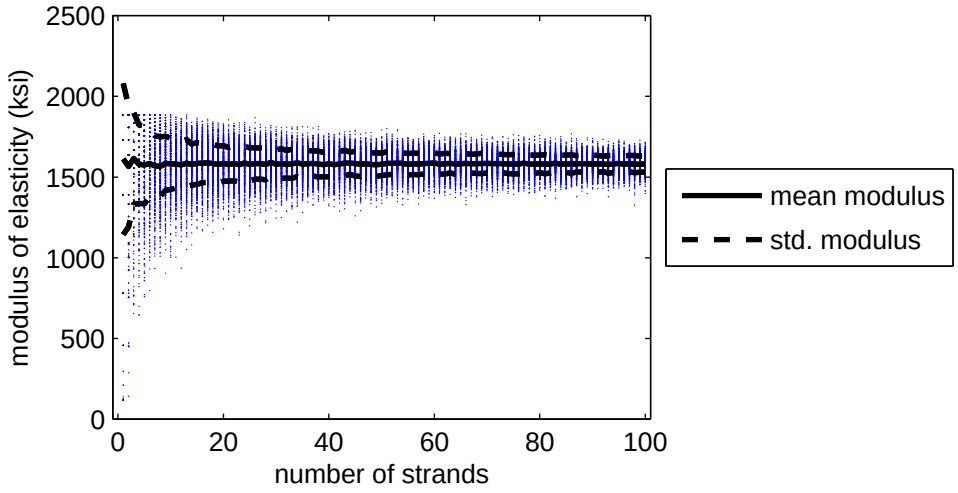

Figure 7.1. As the number of strands are increased in a cross-section the variation of the modulus of elasticity is reduced.

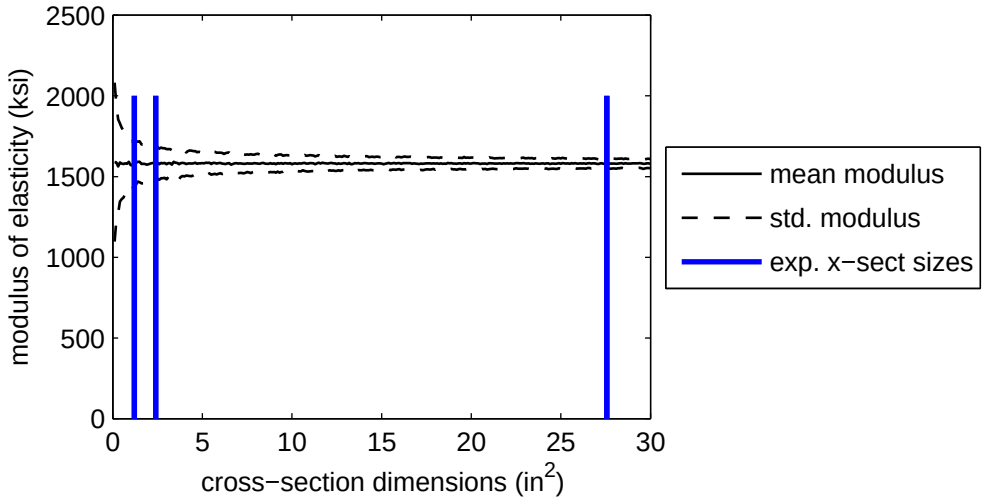

Figure 7.2. The cross-sectional size is important in the determination of characteristics of the modulus of elasticity and its variation.

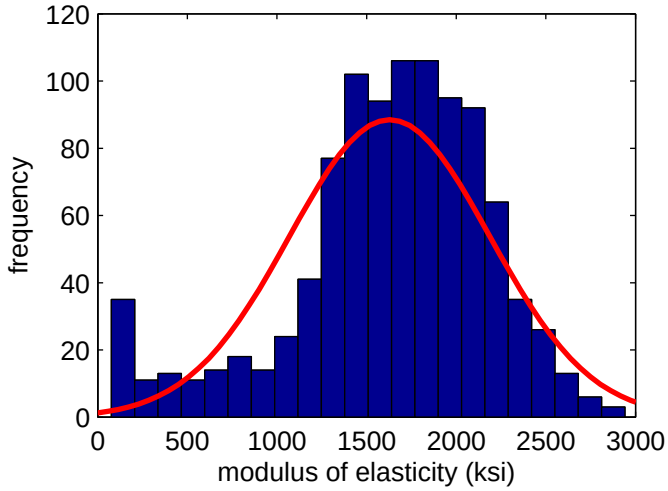

Figure 7.3. 1000 observations of the modulus of elasticity for cross-sections with 1 strand.

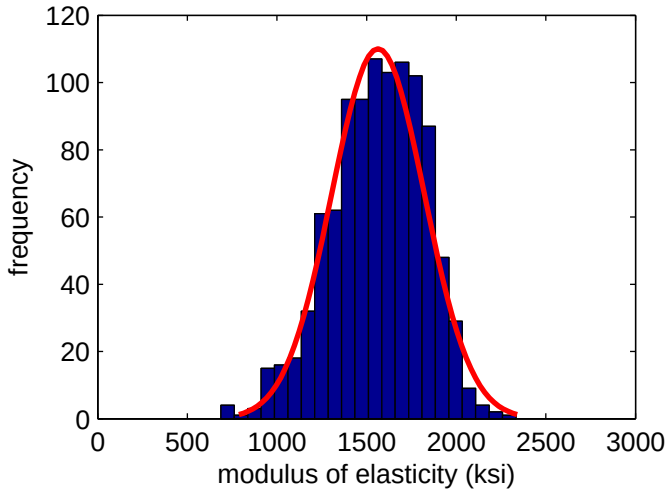

Figure 7.4. 1000 observations of the modulus of elasticity for cross-sections with 5 strands.

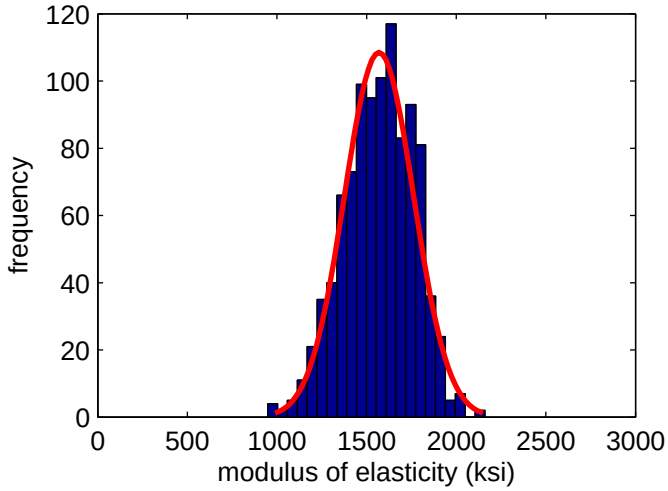

Figure 7.5. 1000 observations of the modulus of elasticity for cross-sections with 10 strand.

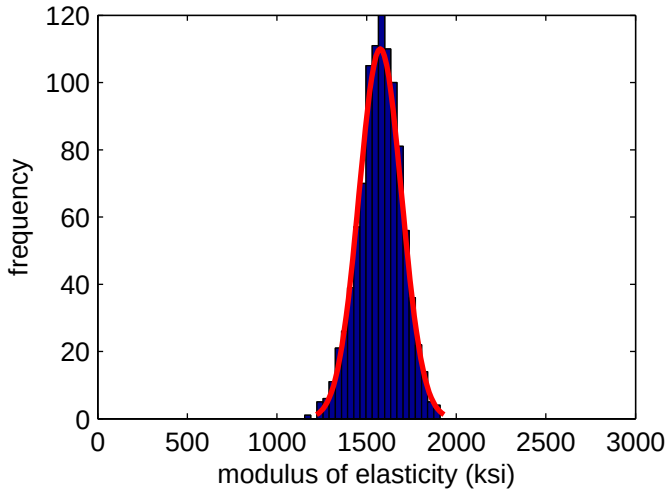

Figure 7.6. 1000 observations of the modulus of elasticity for cross-sections with 50 strands.

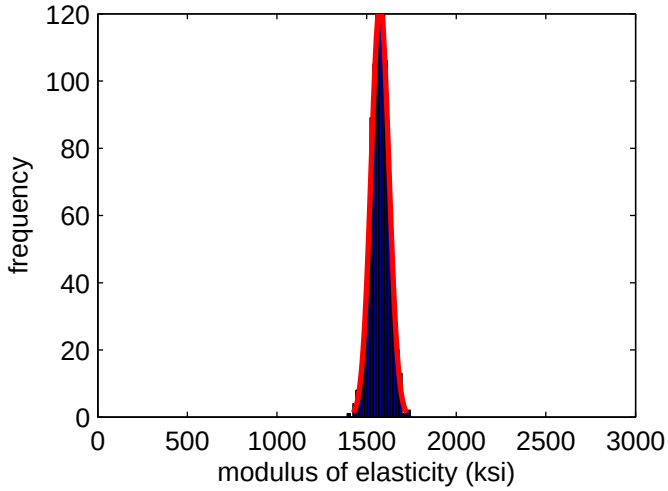

Figure 7.7. 1000 observations of the modulus of elasticity for cross-sections with 150 strands.

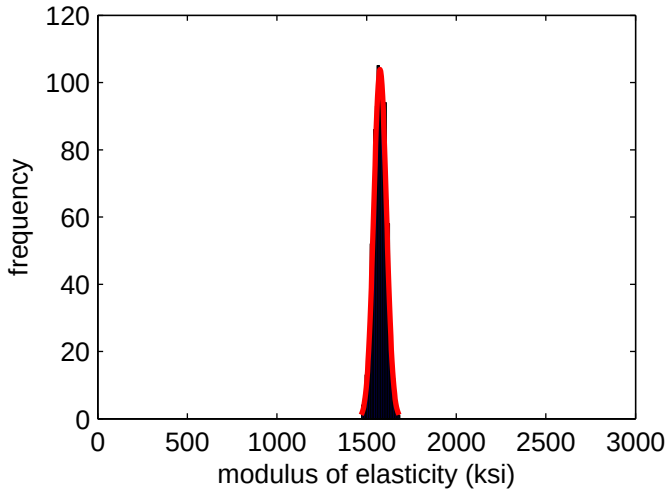

Figure 7.8. 1000 observations of the modulus of elasticity for cross-sections with 300 strands.

in comparison to the modulus of elasticity data. This is due to both the elastic and strength parameters being random. Also, the elastic and strength properties are uncorrelated, which causes data of sections with very few strands to be non-Gaussian because the Central Limit Theorem does not apply to sections of this size. A relationship of the number of strands and standard deviation of the ultimate stress are taken from cross-sections having greater then 15 strands which is

$$\sigma_F = \frac{0.71 \text{ ksi}}{\sqrt{n_s}} \tag{7.3}$$

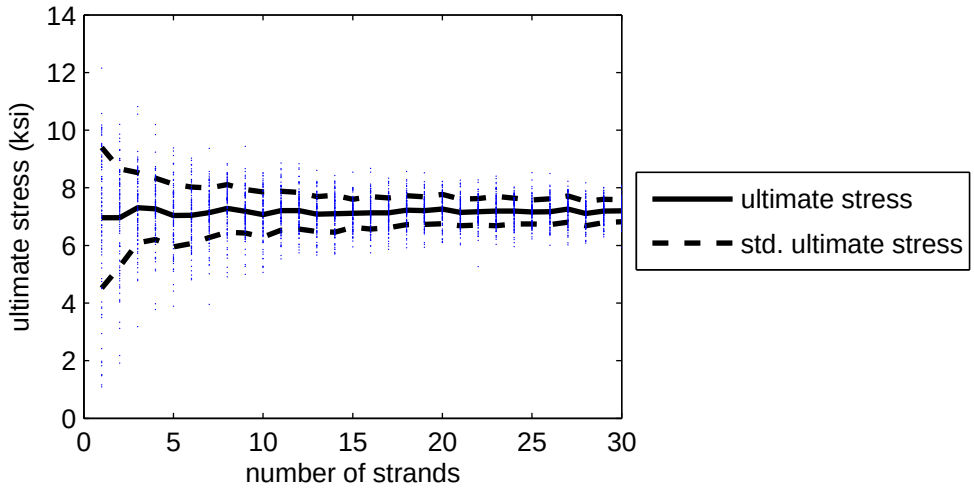

Figure 7.9. As the number of strands are increased in a cross-section the variation of the ultimate stress is reduced.

7.2.2 Study of Grain Angle distributions on the Modulus of Elasticity

To best understand the stiffness characteristics of Parallel Strand Lumber a grain angle distribution must be defined in order to yield meaningful data of the mean and variation of the modulus of elasticity process along the length of a given member. A literature review provided insight into two grain angle distributions for Parallel Strand Lumber.

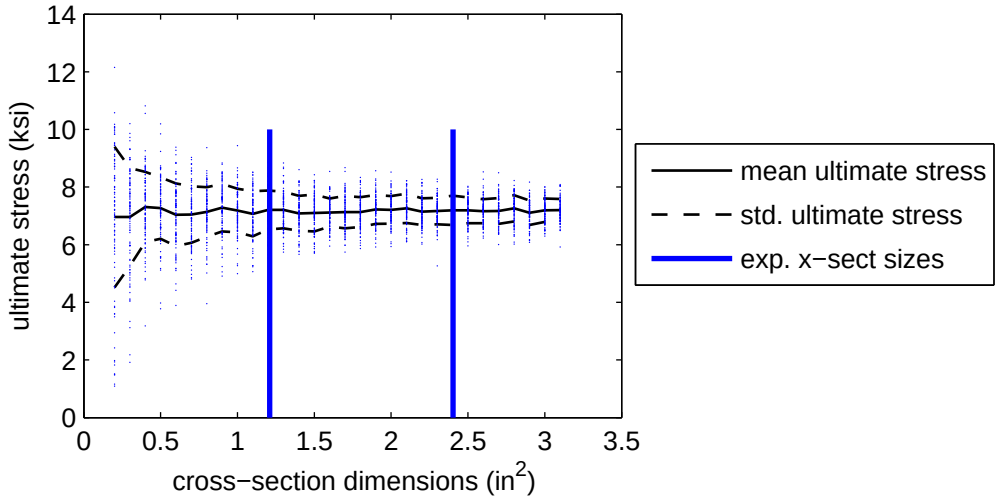

Figure 7.10. The cross-sectional size is important in the determination of characteristics of the ultimate stress and its variation.

Bejo and Lang [3] reported a truncated Gaussian distribution at $\pm 15^o$ which fit both their experimental and simulated data. This grain angle distribution is shown graphically in Figure 7.11. An important note is that this distribution neglects misaligned strands and knots. These factors will be discussed more in depth below.

Clouston [4] reports a grain angle distribution on the scale from 0^o to 90^o of 2366 observations lumped in 5^o or 10^o intervals. The majority of the probability mass is concentrated at 0^o. Even though the majority of the probability mass is concentrated between $0 - 15^o$ similar to Bejo and Lang's distribution approximately 14% of the probability mass is located at higher grain angles which is descriptive of misaligned strands and knots.

To select a probability mass function that will be used throughout all of the simulations, 1,000 simulations were run using both grain angle distributions. The Bejo and Lang distribution yielded a 7% larger mean modulus of elasticity. The standard deviation of the modulus of elasticity is significantly smaller in the Bejo and Lang distribution by 68%. In these simulations the neglect of knots and misaligned

strands does not effect the overall mean modulus of elasticity, but have a significant effect on standard deviation.

When comparing this data to the experimental results, the grain distribution reported by Clouston gives a much better representation of the standard deviation of the modulus of elasticity, which is the justification to why this distribution is used in simulation of Parallel Strand Lumber members in these studies.

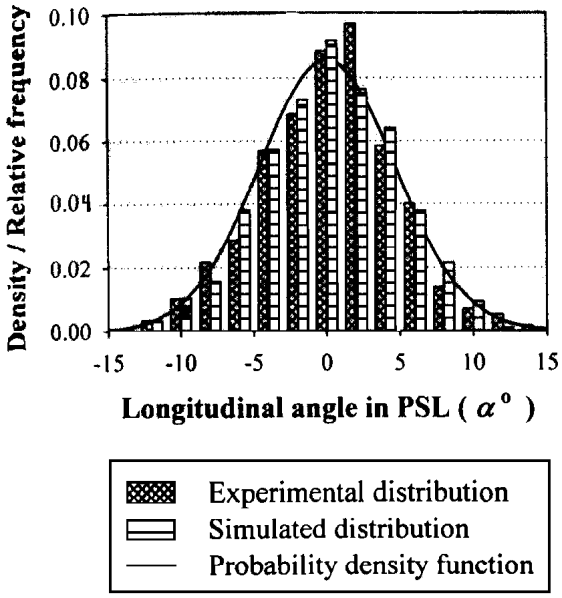

Figure 7.11. Bejo and Lang simulated and experimental grain angle pmf [3]

7.2.3 Study of Defects on the Modulus of Elasticity and Ultimate Stress

The effect defects have on the effective modulus of elasticity and strength of Parallel Strand Lumber is very important when determining factors of safety and quality control on allowable materials. If the effect of defects can be quantified manufacturers can determine safety limits and better predict the mean and standard deviation of effective properties.

From the data generated for the effective modulus and ultimate stress the effect of defects is investigated. Let θ_i be the grain angle of strand i. Strand i contains a

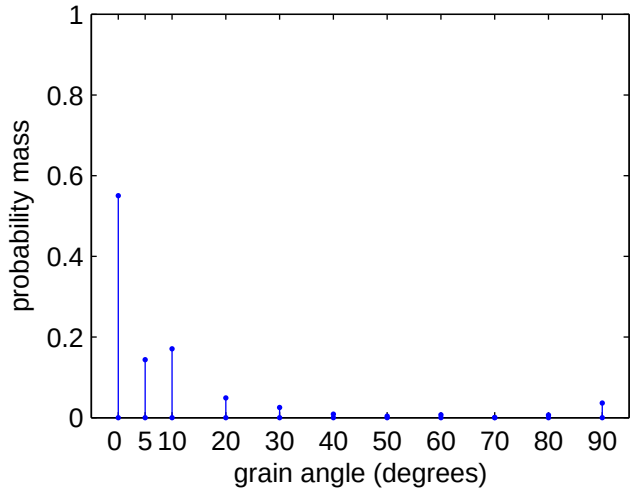

Figure 7.12. Clouston experimental grain angle pmf [4]

defect if $\theta_i \geq \theta_{defect}$, where θ_{defect} is a threshold angle defining a defect or knot. Here $\theta_{defect} = 90^o$ and $\theta_i = 90^o$ is attributed to a knot in the material.

To study the effect of the number of defects on the effective modulus and strength, let ϕ_{defect} be the fraction of strands satisfying $\theta_i > \theta_{defect}$. Let ϕ_{defect} range between 0 and 0.35. As this percentage of defects is increased the cumulative distribution function which is used to sample the grain angle is adjusted by recalculating the probability mass for each grain angle in the pmf given a known percentage of defects and the original pmf. As the number of defects within the member is increased the modulus of elasticity and ultimate stress decreases. As the percentage of defects is increased the variability of the wood composite is also increased. To increase safety it would be optimal to eliminate all defects within each Parallel Strand Lumber member, but this is not very cost effective.

To control serviceability and safety an expression for $\phi_{threshold}$ can be determined from simulated or experimental data where $\phi_{threshold}$ is a quality control value given a desired threshold modulus of elasticity or ultimate stress. $\phi_{threshold}$ is defined as the mean minus n standard deviations. An example data set for the simulated mean

effective modulus of elasticity of a 24 strand compression model with a percentage of defects ranging from [0,35%] is shown in Figure 7.13. Figure 7.14 shows a data set for the ultimate stress.

The standard deviation of the modulus of elasticity and ultimate stress are non linear with an exponent >1 with linear decaying means. Linear fit lines are used for both the mean and standard deviation because for this data a linear fit still yields a good representation and is conservative.

To formulate an expression for $\phi_{threshold}$ trend lines are applied to the mean and standard deviation at each increment of percentage of defect which yields the equation $\mu = \mu_o - c_1\phi_{threshold}$, where μ_o is the mean when the percentage of defects is zero and c_1 is a linear trend constant. The equation for the standard deviation can be similarly written as the equation $\sigma = \sigma_o - c_2\phi_{threshold}$, where σ_o is the mean intercept at X=0 and c_2 is a linear trend constant. The trend line representing the mean minus n standard deviations is written as $\mu - n\sigma = (\mu_o - c_1\phi_{threshold}) - n(\sigma_o - c_2\phi_{threshold})$. The threshold modulus of elasticity or ultimate stress $Y_{threshold}$ is then equal to the expression

$$Y_{threshold} = \mu_o + c_1\phi_{threshold} - n\sigma - nc_2\phi_{threshold}. \tag{7.4}$$

By rearranging and solving for $\phi_{threshold}$ yields

$$\phi_{threshold} = \frac{Y_{threshold} - (\mu_o - n\sigma_o)}{c_1 - nc_2}. \tag{7.5}$$

The 24 strand simulations yield the following model for the modulus of elasticity

$$\phi_{threshold} = \frac{Y_{threshold} - (1630 \text{ ksi} - n84.5 \text{ ksi})}{-15 - n2.1}. \tag{7.6}$$

Similarly, the 24 strand simulations of the ultimate stress yield

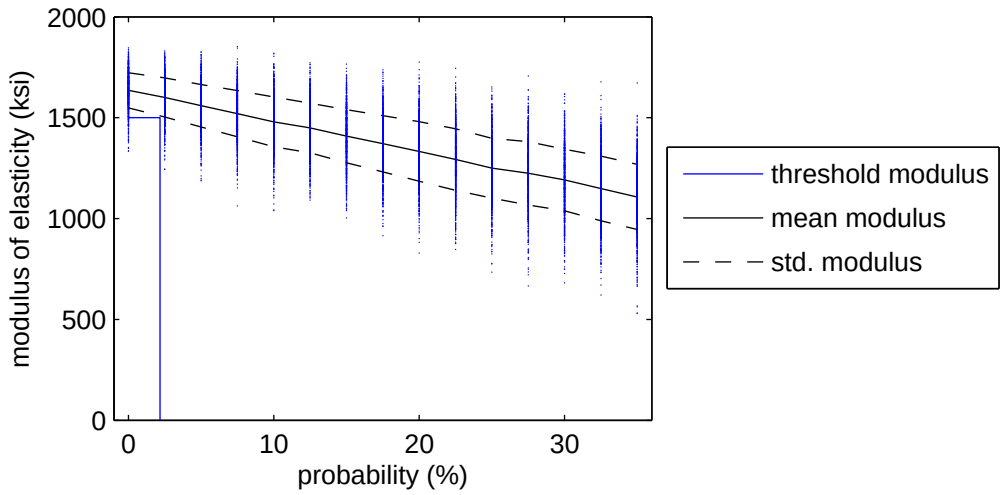

Figure 7.13. 1000 - 24 strand cross-sections for different percentages of detects. As the percentage of defects is increased the variability is increased and modulus of elasticity decreases linearly.

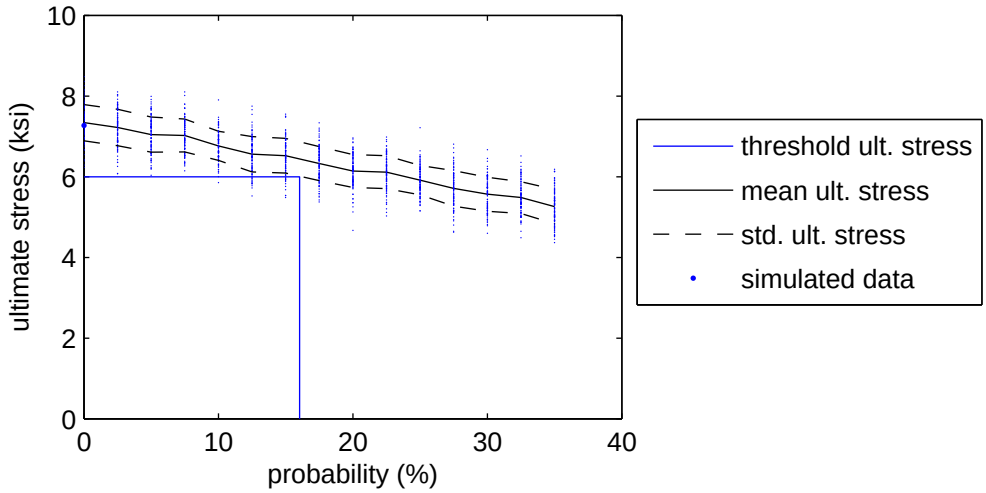

Figure 7.14. 1000 - 24 strand cross-sections for different percentages of detects. The ultimate stress decreases linearly with an increasing percentage of defects although the variation remains nearly constant.

$$\phi_{threshold} = \frac{Y_{threshold} - (7.34 \text{ ksi} - n0.45 \text{ ksi})}{-0.0592 + n0.0008}. \tag{7.7}$$

When comparing Figures 7.13 and 7.14 the standard deviation of the ultimate stress is constant and for the modulus of elasticity it is increasing as the percentage of defects are increased. This cannot be exactly explained, but the reason for this may be because the ultimate stress data for the sample size given is non-Gaussian.

7.3 Finite Element Studies

7.3.1 Finite Element Studies Overview

The finite element method is a powerful tool in research which will allow more insight into the interaction between strands and verify assumptions made for the 2-D computational model. ADINA v8.3.3 [1] is used as a finite element program. The elements used are three dimensional 27 node elements. The material is modeled as orthotropic and the failure model used is Tsai-Hill. Ten time steps were used in each model where three of these time steps were in the linear-elastic regime and the rest were in the plastic and post-plastic regime. The meshing used varied between models. Each mesh is chosen based on a convergence study. Figures 7.15 and 7.16 show mesh convergence studies for the largest compression and bending specimens used. As the mesh size is increased the solutions do not vary by more than 1-3%.

The overall goal of these studies are to allow insight into aspects of modeling that simplified methods could not observe, such as, the interaction of shear forces or failure stress in bending. An in depth analysis is presented in the following two sections with a comparison between the finite element method and simplified method in the concluding remarks of this chapter.

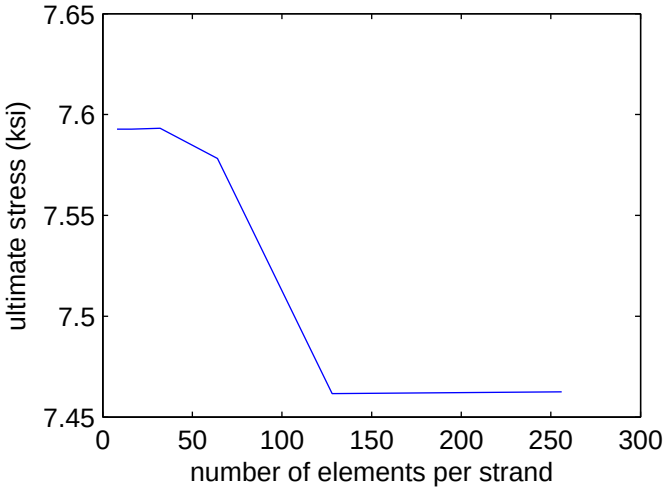

Figure 7.15. Mesh convergence study of the ultimate stress at failure for a uni-axial compression specimen.

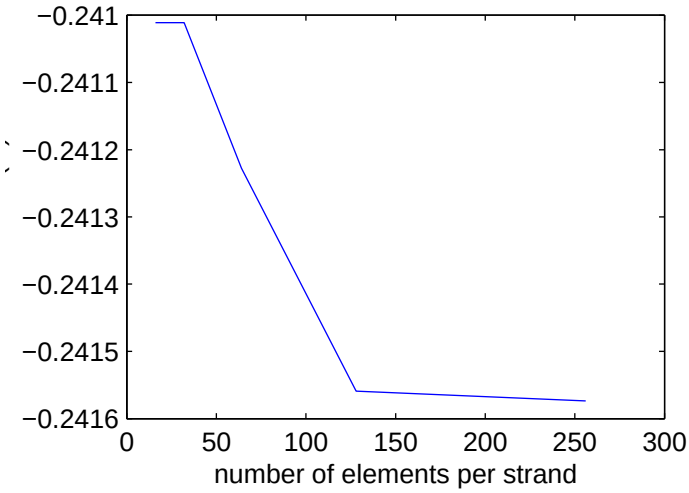

Figure 7.16. Mesh convergence study of the center displacement for a three point bending specimen.

7.3.2 Compression Finite Element Studies

Two cross-sectional sizes which match previous simulation and experimental data are used to estimate the modulus of elasticity and ultimate stress of a member of Parallel Strand Lumber in compression. The finite element model uses three dimensional solid bodies aligned together to represent the strands in a cross-section outlined in more detail in Chapter 2. These three-dimensional bodies allow for interactions that are neglected in other models such as $\sigma_z = \tau_{yz} = \tau_{xz} = 0$, due to the simplification to two-dimensions. The grain angle was modeled using orthotropic axis, which are defined using the previously described deterministic value. This study also helps verify some simplification of other models by obtaining values of the shear and z-axis stresses of given members. At failure the average stresses were σ_z = -0.0039 ksi, τ_{yz} = -0.0038 ksi, and τ_{xz} = 0.033 ksi. These values, while very small, still have an influence on the failure of the cross-section because the capacities in shear are very low.

Figures 7.17 and 7.18 show representations of solved cross-section models for the 1.10 in and 1.55 in models. In Figure 7.18 the top right corner of the cross-section has a very weak strand which varies little to no load. In an actual cross-section this may be where failure occurs first by delamination as the cross-section deforms. From this you can see that the compression stress in the model varies spatially across the cross-section and along the length of the model due to ending strands within the length of a member. The compression stresses are estimated by calculating the reaction forces from a uniform displacement applied at one end. Tables 7.1 and 7.2 show the results of 30 finite element bodies for each cross-section size. Listed in Tables 7.3 and 7.4 are a summary of the experimental results in comparison to the compression results from the finite element and simplified 2-D compression models. The finite element model captures the variation and mean of the modulus of elasticity and ultimate stress much better than the simplified model. This is because the assumption of constant strain across the cross-section and along the member is not valid. Figures 7.19 and 7.20

show how the strain varies along the length and across a given section. Two locations where strands are ending in the cross-section have a large influence on the local strain around these locations. The strain on the side located near the boundary conditions is nearly zero and on the side closer to the load application the strain is very high. Even when ignoring these strands ending, the variation caused by strands having different stiffness values causes significant variation through the cross-section. This varying strain field results in more accurate results than the 2D simplified model. The average shear forces in the body at failure of the finite element model are small they still have an effect on the calculated effective properties. These shear forces are τ_{yz} = -0.0038 ksi and τ_{xz} = 0.033 ksi. The shear strengths are very small, so even these small shear forces still have an effect on the ultimate stress of the specimen. The cross-correlation of the modulus of elasticity and ultimate stress is 0.20 for the A specimens and 0.55 for the B specimens. This large difference may be due to the relatively low number of specimens generated or possibly a size effect.

Although the finite element model yields very good results and more detailed models in comparison to the simplified model the computational time is approximately 10-20x greater in the finite element model. As the size of the model gets longer more elements are used per strand which changes aspects of the post processing commands. As the size of the cross-section increases the displacement time stepping must also be adjusted in such a way as to allow estimations of strain and stress in the linear elastic range and plastic range.

Table 7.1. Finite element estimates of the stresses at failure for 30 - 1.10 in x 1.10 in x 3.25 in cross-sections and estimates of the modulus of elasticity.

	stress-YY	stress-XX	stress-ZZ	stress-YX	stress-YZ	stress-XZ
mean (ksi)	-0.0059	7.36	-0.0068	-0.0006	-0.0008	0.0023
std. dev. (ksi)	0.0048	0.60	0.0039	0.0071	0.0038	0.033

Table 7.2. Finite element estimates of the stresses at failure for 30 - 1.55 in x 1.55 in x 5.00 in cross-sections and estimates of the modulus of elasticity.

	stress-YY	stress-XX	stress-ZZ	stress-YX	stress-YZ	stress-XZ
mean (ksi)	-0.0006	7.39	-0.0019	0.0005	-0.0003	0.0023
std. dev. (ksi)	0.0036	0.40	0.0032	0.0078	0.0014	0.016

Table 7.3. Finite element estimates of the modulus of elasticity.

	FE Group A	FE Group B
mean (ksi)	1780	1890
std. dev. (ksi)	231	217

Table 7.4. Finite element observations of the ultimate compressive strength for specimen groups A and B with a comparison to the experimental and simplified model data.

	FE A	FE B	virt. A	virt. B	exp. A	exp. B
mean (ksi)	7.36	7.39	7.19	7.18	7.71	8.97
std. dev. (ksi)	0.60	0.40	0.20	0.25	1.09	1.02

7.3.3 Bending Finite Element Studies

Two specimen sizes, where one of the specimen sizes matches experimental data, are chosen to observe the bending modulus of elasticity. Also discussed in this section are ways to gather data on the bending stress at failure of a cross-section. The bending tests are performed in accordance to Chapter 2. Three dimensional solid bodies are used to represent strands. Randomly distributed strand lengths could not be implemented where they were in the compression finite element studies due to the

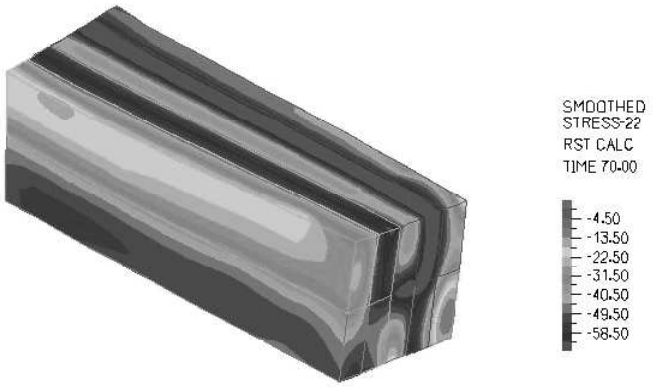

Figure 7.17. Sample finite element 1.10 in x 1.10 in x 3.25 in body, subject to uni-axial compression.

Figure 7.18. Sample finite element 1.55 in x 1.55 in x 5.00 in body. The top right corner of the cross-section has a very weak strand which carries little to no load.

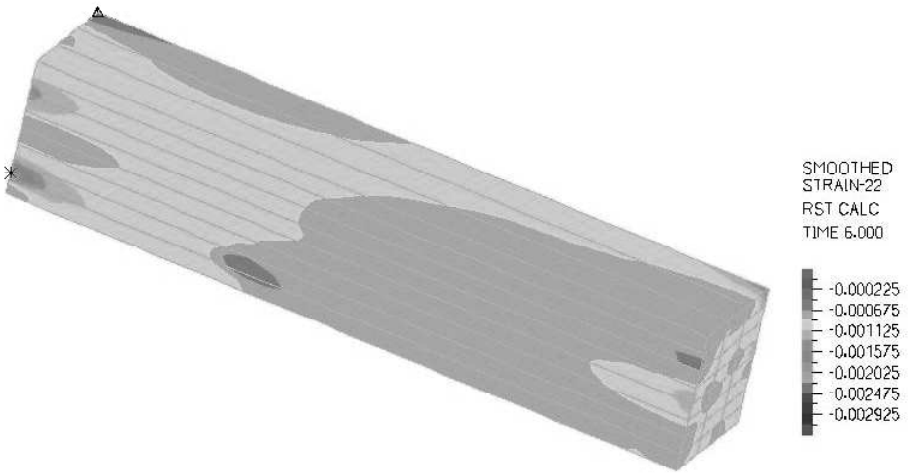

Figure 7.19. Sample finite element 1.55 in x 1.55 in x 5.00 in section. The strain field is in the elastic range which shows that the assumption in the 2D model of constant strain is not valid. The strain at certain locations in the cross-section can vary significantly depending on the constitutive elastic properties. A location where a strand ends and a new strand begins is shown. This causes a localized strain to be observed.

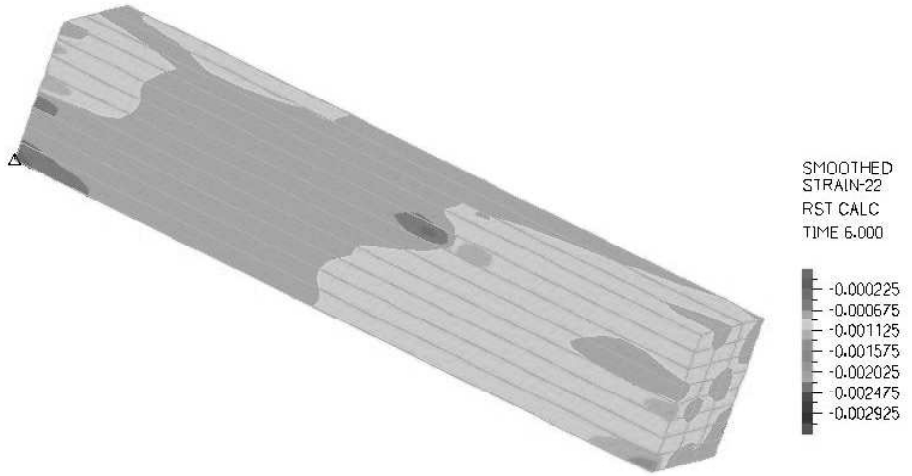

Figure 7.20. A second location where a strand ends and a new strand begins is shown. This causes a localized strain to be observed.

Table 7.5. Finite element observations of the modulus of elasticity in compression for specimen groups A and B with a comparison to the experimental and simplified model data.

	FE A	FE B	virt. A	virt. B	exp. A	exp. B
mean (ksi)	1780	1890	1580	1573	1840	1860
std. dev. (ksi)	231	217	174	120	300	400

placing of loads and boundary conditions so the strand lengths are set to match the overall model length. The reasons the strand length is set equal to the model length are complications arose in the placing of the load. The load needed to be applied at subdivisions in the center of the member. Lengthwise variability made it nearly impossible and computationally expensive to accurately divide strands so there would be a subdivision located exactly at the center line in the bending member. Also, the introduction of having random lengths associated with strands and extra subdivisions would cause the node numbering system to change. The nodes where the deflections are measured to calculate the modulus of elasticity are taken at a location at the center line of the bending specimen on the bottom face. If more strands were introduced the location of these nodes would have to be determined via data post processing before results could be post processed. This drastically increases the computational time and expenses in comparison to the current finite element model where these node locations can be easily read by hand once off an initial model and inputted into the program to simulate any number of cross-sections. Also, due to computational limits on the amount of physical memory available the only cross-sections that could be readily calculated are short bending specimens with a small cross-section to limit shear deformations. Large cross-sections such as the 5.25 in x 5.25 in x 96 in could not be calculated because the amount of memory needed exceeded the capacity of the server used to run these simulations.

Two specimen sizes, one, a 24 strand - 1.55 in x 1.55 in x 15 in section and the other, a 40 strand - 2 in x 2 in x 38 in specimen, are simulated using the above

finite element algorithms. The number of observations is 30 for each cross-sectional size with the results shown in Table 7.6 with a comparison to the experimental data. Figures 7.21 and 7.22 show progressive yielding of a section and the corresponding increasing stress. Observations of this yielding indicate it is very subjective to when a cross-section actually fails, which is only evident in computational models. In each of these four figures the load is increasing by a constant amount. The results of these simulations coincide with experimental and previous simulated data using the simplified method. The finite element model yields a similar estimate of the bending modulus of elasticity compared to the simplified simulation method when compared to the experimental 1.55 in x 1.55 in cross-sections. The simplified method yields much better estimations of the variability. This is because the simplified method allows variable strain lengths to be used. Also, yielding and high stresses occur at the load application because loads are applied at nodes which is unrealistic and causes large stress concentrations. The second set of finite element simulations were performed to gather another estimate of the variation and modulus of elasticity when increasing the cross-sectional size. The modulus of elasticity and variation are very similar in both cases, although the variation is only based on 30 observations compared to 1000 of the simplified method. The variation is similar to the experimental in all cases, where the difference in variation is most likely due to the neglect of within strand variation and the inability to implement strands of different lengths.

Observations of the load at which failure initiates in these models is very subjective. The simulations are designed to limit the number of time steps. The objective of the bending model is to gather several elastic measurements and then observe the progressive yielding to failure of the cross-section. Due to the cross-sections having random elastic and strength properties failure occurred at different stresses for every cross-section. Strands with a high grain angle would fail very soon under the loading when the cross-section would still behave elastically. Current strength models in the

finite element software are very good for strands in compression. In bending some strands experience tensile stress, some experience compression stresses, and strands located near the neutral axis experience both stresses [4]. Due to the mixed stress conditions a new failure criteria must be developed and implemented to get the load at which failure occurs in bending.

Table 7.6. Bending test results. The script s stands for the short bending specimens which matched the experimental length of 8 ft. The l script denotes the long 640 ft samples.

	FE A	FE B	sim. A-s	sim. A-l	exp. A
mean (ksi)	1620	1655	1572	1572	1648
std. dev. (ksi)	97.1	97.5	94	111	150

7.3.4 Finite Element Conclusions and Recommendations

Finite element solutions are powerful tools to observe the response of Parallel Strand Lumber in bending and compression. These methods are computationally expensive, but provide much insight into interactions a simplified method neglects. In compression the finite element model shows the strain varies within the cross-section and along the length of a member which yields much better results for the variability and ultimate compressive strength in comparison to simplified 2D models. The finite element model verifies the assumption the shearing stresses and through-thickness stresses are negligible in uni-axial compression. Even with some twisting and bending of these cross-sections, which was also noticed in the experiments, the resulting forces are very small but can not be ignored. Overall, the results of the finite element model are significantly more accurate and more representative of an actual model in comparison to a simplified models described in previous chapters.

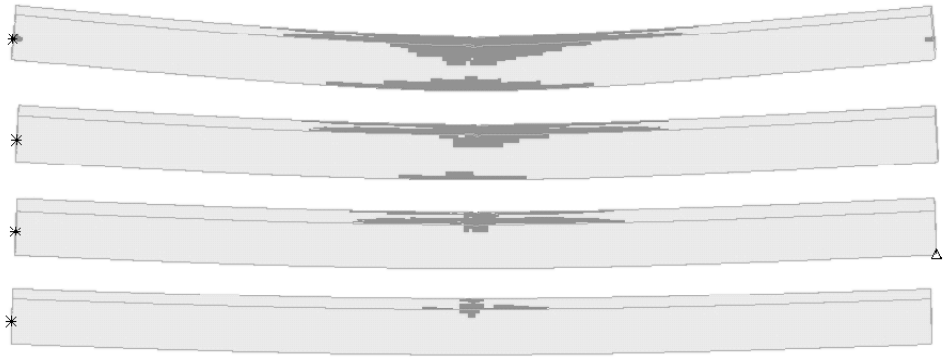

Figure 7.21. Progressive yielding of a 40 strand 2 in x 2 in cross-section. The time increases from bottom to top.

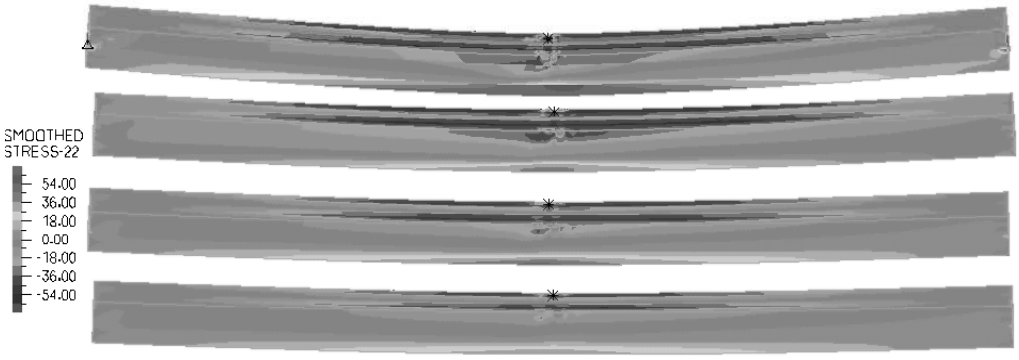

Figure 7.22. The resulting stresses from the progressive yielding of a 40 strand 2 in x 2 in cross-section. The time increases from bottom to top.

The bending models are significantly more computationally expensive in comparison to short and small compression specimens because the members total length and size are significantly longer and larger. It is also very hard to implement many features of Parallel Strand Lumber, such as, length-wise variations or proper fracture mechanics models in the bending model. In comparison to the finite element model, the simplified models provide much faster and easier to implement solutions to a bending problem. Also, large specimens, such as those that would be used for commercial products, require more sophisticated finite element methods to reduce the amount of time it would take to solve. The simplified models can take any cross-sectional size and length as input and provide a fast and more detailed solution, such as, providing length-wise variability measurements.

Overall, the finite element method is a very accurate and easy way to gather observations of the compressive modulus of elasticity and ultimate stress at failure. The simplified models though provide easy to implement and accurate results in bending where the finite element method is very computationally expensive and lacks many actual features of Parallel Strand Lumber.

CHAPTER 8

CONCLUSIONS

Three point bending tests at a series of locations along the length of Parallel Strand Lumber of two different size cross-sections and a series of compression tests of a divided longer member provides measurements of a spatially varying modulus and ultimate stress field. These experimental results show that the variation of Parallel Strand Lumber is approximately 50% lower then that of dimension lumber due to the averaging of material properties for nominally sized members.

Results indicate that lumber specimens in typical machined lengths and cross-sections are not long enough to provide a reliable estimation of the spatial variation of material properties unless there is a large enough sampling pool to estimate ensemble statistics. Sample estimates of the correlation length for the modulus of elasticity in bending and compression and the ultimate compressive strength are of the order ten inches. By taking ensemble estimates of these statistics the correlation length is 56 in.

Models are developed which rely on a simplified treatment of the Parallel Strand Lumber mesostructure. Finite element models are also created to verify and compare to these simplified models. Both models include uncertainty in the orthotropic constitutive elastic constants, grain angle, strand length, and failure criteria. The simplified models provide samples of the elastic modulus in bending and compression and the ultimate stress in compression which are analogous to the experimental data through applying a filtering process, which is similar to the averaging of test, to the

unfiltered processes. The filtered process is the result of the averaging of material properties between two support locations in a three point bending test.

The simplified computational model is verified by comparing first and second moment properties to the experimental results. These models perform well in comparison to the three point bending results with a slight under prediction of the variation of the modulus process. This under prediction is from sources of experimental error and simplification of some uncertainty in the modeling of the mesostructure. The compressive modulus of elasticity does not perform well in comparison to the experimental data. This difference is due to testing methods which do not perform well with Parallel Strand Lumber. The strain is measured from an extensometer, which is attached to the side of the member. This extensometer did not yield very accurate results due to debonding and bending of the outer strands which caused the extensometer to yield false readings. The method of extracting the modulus of elasticity from the stress-strain curves also introduced significant operator error.

The model of the ultimate stress in compression is in good agreement with experimental data with some under prediction of the variation of the ultimate stress field. The finite element model is in better agreement by capturing the variation of the modulus of elasticity and ultimate stress much better then the simplified models. For the 2-D simplified models constant strain was assumed throughout the member. The finite element model showed that the strain varied significantly within the cross-section and along the length of the member. Due to this simplification not being valid the finite element model yielded much better results then the simplified models. Aside, the simplified model's assumption of neglecting shear and through-thickness forces was observed in the finite element results. The prediction of variation and mean of these effective properties agreed with experimental data with slight under predictions due to the errors mentioned above. The three point bending finite element models had slightly worse agreement then the simplified method results. The three

point bending finite element model is very hard to implement all the key features of Parallel Strand Lumber, such as strand length variation. This model is also very computationally expensive and not recommended. The simplified three point bending model is much faster, easier to implement, more user-friendly, and yields better estimations of the mean and variation of the modulus of elasticity.

For the simplified bending model when there are approximately 10-50 strands in a cross-section with a short test span the unfiltered and filtered modulus of elasticity processes converge. When there are more than approximately 100 strands in a cross-section there is significant averaging where bending tests do not provide accurate measurements of the variation of the elastic modulus process.

The distribution of the compression modulus of elasticity, bending modulus of elasticity, and ultimate stress are Gaussian when there are more than approximately 15 strands in the cross-section. If there are less than 15 strands in the cross-section these processes are non-Gaussian because of the small sample size of strands. The modulus of elasticity in these cross-sections is independent of the number of strands in the cross-section. The variation of the effective properties scales inversely with the number of strands. The auto covariance can be modeled as a linear decaying process to zero.

Additional studies suggest that finite element method should be used to model the compression specimens because they provide better estimations, otherwise, more development of the simplified model is needed. The simplified model does perform very well for three point bending specimens where the finite element is computationally expensive and very hard to implement. The simplified models in both compression and bending provides fast, accurate, user-friendly estimations of the spatially varying processes, where as the finite element models can only provide point statistics of one sample. The finite element models are also not user-friendly taking significant time to calibrate meshing, time stepping, and the post processing of data. Overall,

the simplified method is proven to provide very easy and accurate estimations of the statistics of Parallel Strand Lumber.

These additional studies also give details on what type of distributions should be used for the grain angle. Two grain angle distributions, one a truncated Gaussian distribution [3], and the other an empirical distribution for observations are presented [4]. A truncated Gaussian distribution does not capture the effect knots or misaligned strands have on the cross-section. These defects drastically reduce the modulus of elasticity and strength of a cross-section. Also, this limits the amount of variation of Parallel Strand Lumber, which is inherently much greater when comparing the computational estimates to experimental data.

In addition to these findings a defect sensitivity parameter study is performed. The modulus of elasticity and ultimate stress of cross-sections containing a varying percentage of defects, or strands which have a grain angle equal to 90^o are estimated. This gives insight into code based design on factory limits on what types of materials are used in the making of Parallel Strand Lumber.

The objective of this master's thesis research is to successfully implement easy and accurate simplified models that can predict important characteristics and properties such as the ultimate stress or modulus of elasticity of compression and bending members. These models then can be used to give estimations of the effective properties of new composites, which may reduce or limit the number of expensive and time consuming experimental tests needed.

BIBLIOGRAPHY

[1] Automatic dynamic incremental nonlinear analysis. Version 8.3.3. 1994-2004 ADINA R & D Inc.

[2] ASTM. Standard methods of statis tests of lumber in structural sizes. American Society for Testing and Materials D 198–05.

[3] Bejo, L., and Lang, E. Simulation based modeling of the elastic properties of structural composite lumber. vol. 36, pp. 395–410.

[4] Clouston, P. Characterization and strength modeling of parallel strand lumber. *Holzforschung 61* (2006), 392–399.

[5] Clouston, P., and Lam, F. Computational modeling of strand-based wood composites. *ASCE Journal of Engineering Mechanics 127* (2001), 884—851.

[6] Clouston, P., and Lam, F. A stochastic plasticity approach to strength modeling of strand-based wood composites. *Composites Science and Technology 62* (2002), 1381–1395.

[7] Ekevad, M. Method to compute fiber directions in wood from computed tomography images. *Journal of Wood Science 50* (2004), 41–46.

[8] Green, D., Winandy, J., and Kretschmann, D. Wood handbook. Forest Products Laboratory, Madison, WI.

[9] Hu, Y., and Wang, F. Nondestructive test and prediction of modulus of elasticity of veneer-overlaid particleboard composite. *Wood Science and Technology 39* (2005), 439–447.

[10] Lam, F., and Varoglu, E. Variation of tensile strength along the length of lumber part 1: Experimental. *Wood Science and Technology 25* (1991), 351–359.

[11] Lam, F., and Varoglu, E. Variation of tensile strength along the length of lumber part 2: Model development and verification. *Wood Science and Technology 25* (1991), 449–458.

[12] Liu, Y., and Lee, A. Selected properties of parallel strand lumber made from southern pine and yellow-poplar. *Holzforschung 57* (2003).